Eastern Atlantic deep-water circulation and carbon storage inferred from neodymium and carbon isotopic compositions over the past 1.1 million years

Tachikawa Kazuyo, William Rapuc, Laurence Vidal, Quentin Dubois-Dauphin, Thomas Westerhold, Abel Guihou, Torsten Bickert, José Pérez-Asensio, Pierre Deschamps, Charlotte Skonieczny

Eastern Atlantic deep-water circulation and carbon storage inferred from neodymium and carbon isotopic compositions over the past 1.1 million years

Kazuyo Tachikawa [a, *], William Rapuc [a, b], Laurence Vidal [a], Quentin Dubois-Dauphin [a], Thomas Westerhold [c], Abel Guihou [a], Torsten Bickert [c], José N. Pérez-Asensio [a], Pierre Deschamps [a], Charlotte Skonieczny [d]

[a] *Aix Marseille Univ, CNRS, IRD, INRAE, Coll France, CEREGE, Aix-en-Provence, France*
[b] *Environment Dynamics and Territories of Mountains (EDYTEM), Université Savoie Mont Blanc, CNRS, 73000, Chambéry, France*
[c] *MARUM, University of Bremen, 28359, Bremen, Germany*
[d] *Université Paris-Saclay, CNRS, GEOPS, 91405, Orsay, France*

ABSTRACT

The Mid-Pleistocene transition (MPT; 1200 to 800 thousand years, kyr) is marked by the shift from 41-kyr to 100-kyr interglacial-glacial cyclicity without substantial change in the astronomical forcing. This change in climate response relied on internal feedback processes including interaction between ice sheet/sea ice, ocean circulation and the carbon cycle. It was suggested that a major perturbation of global oceanic carbon chemistry occurred at around 900 ka (Marine Isotope Stage, MIS, 24–22) although the mechanism responsible for the change is still to be elucidated. To investigate the link between the Atlantic Meridional Overturning Circulation (AMOC) and oceanic carbon storage for the past 1100 kyr, we combined neodymium isotopic composition ($^{143}Nd/^{144}Nd$ or ε_{Nd}) recorded in foraminiferal authigenic fractions with epibenthic foraminiferal $\delta^{13}C$ and $\delta^{18}O$ from two cores in the North- and South-east Atlantic Ocean. Glacial/interglacial ε_{Nd} amplitude is smaller before the 900-ka event than after the event. The 900-ka event is marked by increase in seawater ε_{Nd} at both sites. These observations are consistent with previous studies, suggesting basin-wide ε_{Nd} changes. Combined with existing data, these new results reveal a persistent meridional gradient of seawater ε_{Nd} in the Atlantic Ocean over the past 1100 kyr. By comparing the reconstructions with numerical modelling results, we propose that weaker AMOC and changes in Nd sources to the North Atlantic were the main reasons for the observed ε_{Nd} shift at the 900-ka event in relation to the evolution of the Northern hemisphere cryosphere. The influence of enhanced Southern Ocean overturning circulation on ε_{Nd} values was estimated to be minor. Seawater ε_{Nd} and benthic $\delta^{13}C$ relationship for the whole study period indicates the presence of carbon-rich glacial deep water (>3000 m) in the North and the South Atlantic, in particular at MIS 22 and 24. This suggests that, in addition to weaker AMOC, reduction of deep-water ventilation and/or air-sea exchange in the Southern Ocean could have been responsible for the observed low benthic $\delta^{13}C$ values. Together with increased biological productivity due to iron fertilization in the Southern Ocean, the physical process significantly contributed to the deep Atlantic carbon storage during the 900-ka event and the subsequent glacial periods.

1. Introduction

The Mid-Pleistocene transition (MPT; 1200 to 800 thousand years, kyr) is marked by an intensification of glacial/interglacial amplitude and a shift of climate cycle from 41 kyr to 100 kyr (Clark et al., 2006; Chalk et al., 2017). Since the observed changes cannot be explained by variation in solar insolation alone, internal feedback processes should have played a key role. The Atlantic Meridional Overturning Circulation (AMOC) is defined as zonally

integrated surface and deep currents in the Atlantic, and considered to have contributed to such feedback processes (Clark et al., 2006; Pena and Goldstein, 2014; Lear et al., 2016; Farmer et al., 2019).

Several hypotheses have been proposed to explain the origin of the MPT and it is generally accepted that ice sheet dynamics played a fundamental role. Progressive glacial erosion of regolith led to the exposure of hard bedrock, increased the basal stability of ice sheets, and allowed the growth of thicker ice sheets (regolith hypothesis; Clark et al., 2006; Clark and Pollard, 1998; Tabor and Poulsen, 2016). Thicker ice sheets contributed to gradual global cooling across the MPT by intensification of atmospheric circulation because of enhanced latitudinal temperature gradient and active upwelling (Ford et al., 2016; McClymont et al., 2013; Snyder, 2016). Global glacial sea surface cooling, in turn, promoted the climate feedbacks via activation of sea-ice switch (Gildor and Tziperman, 2000). Moreover, the transition from the 40 kyr to the 100 kyr world was accompanied by a decline in minimum atmospheric CO_2 concentrations during glacial maxima (Yan et al., 2019) although available reconstructions of atmospheric CO_2 are still at low temporal resolution (Chalk et al., 2017; Dyez et al., 2018; Higgins et al., 2015; Hönisch et al., 2009). Recently, a combination of ice sheet stabilization with atmospheric CO_2 reduction via biological carbon pumping was proposed to be fundamental to explain the changes observed across the MPT (Chalk et al., 2017; Willeit et al., 2019).

In addition to biological carbon pumping, ocean dynamics affect marine carbon storage. Significant changes in ocean circulation over the MPT were suggested by benthic foraminiferal $\delta^{13}C$ records (Hodell et al., 2003a; Raymo et al., 1990, 1997, 2004; Venz and Hodell, 2002). A decrease in glacial benthic $\delta^{13}C$ values in the Atlantic at the onset of the MPT was interpreted as a weaker formation of North Atlantic Deep Water (NADW) (Raymo et al., 1990), stronger influence of Circumpolar Deep Water (CDW) (Raymo et al., 2004) and/or stagnant ventilation in the deep water of the Southern Ocean (Hodell et al., 2003a). In particular, the 900-ka event (Marine Isotope Stages, MIS, 24 to 22) is characterised by very low $\delta^{13}C$ values in the North and South Atlantic (Hodell et al., 2003a; Raymo et al., 1997) and by an increase in nutrient content and corrosivity of Atlantic waters deeper than 3000 m (Farmer et al., 2019; Lear et al., 2016). The origin of the negative $\delta^{13}C$ excursion and its potential link with deep water circulation, cryosphere evolution and carbon cycle still require clarification.

Seawater Nd isotopic composition ($^{143}Nd/^{144}Nd$ or ε_{Nd}) recorded in authigenic fractions associated with foraminiferal tests provided new constraints on circulation changes. Previous studies measured foraminiferal ε_{Nd} values on three cores from the Southeast Atlantic Ocean to evaluate the relative proportion of northern source water (NSW) and southern source water (SSW) over the MPT (Farmer et al., 2019; Pena and Goldstein, 2014). Based on foraminiferal ε_{Nd} values, a major reduction of NSW proportion was estimated in the Southeast Atlantic between MIS 25 and MIS 21 (Farmer et al., 2019; Pena and Goldstein, 2014). This finding has shed light on the state of the AMOC across the MPT but it is based on records having limited spatial coverage (the white stars in Fig. 1a and b). Moreover, the observed lower NSW proportion could be produced by either weakening of NADW formation or enhanced deep water formation in the Southern Ocean although physical mechanisms are different (Farmer et al., 2019).

In this study, we present new foraminiferal ε_{Nd} records from the Northeast (core MD03-2705; 18°06′N, 21°09′W, 3085 m water depth) and Southeast Atlantic (Ocean Drilling Program, ODP, Site 1085; 29°22′S, 13°59′E, 1713 m water depth) over the past 1100 kyr. Epibenthic foraminifera, *Cibicidoides wuellerstorfi*, $\delta^{13}C$ and $\delta^{18}O$ data were also acquired at ODP Site 1085. Since the location of core

MD03-2705 is under the influence of Saharan dust supplies (Skonieczny et al., 2019 and references therein), some cleaning tests were conducted to examine the fidelity of foraminiferal ε_{Nd} values as a tracer of water mass provenance. ODP Site 1085 is located in the southern Benguela region that might be affected by the past migrations of the upwelling centre (Wefer et al., 1998). To assess the potential influence of local productivity on benthic foraminiferal $\delta^{13}C$ record, authigenic uranium (U) precipitated on foraminiferal tests (Boiteau et al., 2012; Lear et al., 2016) was analysed for ODP Site 1085 samples.

We aim at clarifying reasons for seawater ε_{Nd} variability and possible link to the ocean carbon cycle. A PANDORA 10-box model calibrated with modern Nd compilation (Tachikawa et al., 2017) is used to examine different scenarios affecting seawater ε_{Nd} distribution. Then, the combination of foraminiferal ε_{Nd} with *C. wuellerstorfi* $\delta^{13}C$ allows distinguishing changes in water mass mixing from ventilation changes, and consequent storage of respired carbon in the ocean.

2. Modern intermediate and deep-water circulation in the eastern Atlantic Ocean

The water mass structure in the modern eastern Atlantic Ocean is recognised by a latitudinal salinity transect (Fig. 1). NADW flows southwards in the western Atlantic and bifurcates at around 10°N and at the equator, then enters the eastern basin (the orange arrows in Fig. 1a). The main branch of NADW continues to flow in the western Atlantic and deflects eastwards at approximately 40°S (Larqué et al., 1997) (Fig. 1a). The core of salty NADW is found at 2000−3000 m water depth in the Northeast Atlantic (Fig. 1b). NADW intersects northward flowing Upper and Lower CDW (UCDW and LCDW with the light and dark green arrows, respectively in Fig. 1a) characterised by lower salinity (Fig. 1b). CDW is formed by mixing of NADW, Indian deep water, Pacific deep water as well as locally formed dense waters (Weddell and Ross deep waters; Talley, 2013). The properties of UCDW and LCDW are modified during the northward trajectory by mixing with underlying or overlaying NADW. LCDW occupies essentially the deep Cape Basin (Fig. 1c) at water depths deeper than 3500 m (Dickson et al., 2008). The lower part of LCDW is mixed with the upper part of Antarctic Bottom Water (AABW, the black arrow in Fig. 1a) (Orsi et al., 1999). AABW is formed by brine rejection during sea ice formation in polynyas and in sea ice zone or by super-cooling of ice shelf water beneath the Antarctic ice shelves (Krueger et al., 2012). AABW entering the Atlantic basin is already mixed into LCDW in the Scotia Sea (Naveira Garabato et al., 2002). Another southern source water mass is Antarctic Intermediate Water (AAIW) that is marked by the lowest salinity along the section, flowing northward at 700−1000 m water depths (Fig. 1b).

According to the temperature-salinity diagram and the properties of the different water masses defined by Larqué et al. (1997), core MD03-2705 location is currently bathed in NADW whereas ODP Site 1085 is influenced by LCDW and NADW (Fig. 1c).

3. Materials and methods

3.1. Core material

Core MD03-2705 was retrieved on a seamount about 500 km off the Mauritanian coast in the eastern tropical Atlantic (Fig. 1a) to avoid laterally transported sediment accumulation by bottom currents and massive contribution of river sediments. The core is composed of biogenic carbonates (foraminifera and coccoliths) and terrigenous fraction mainly consisting of Saharan dust (Jullien et al.,
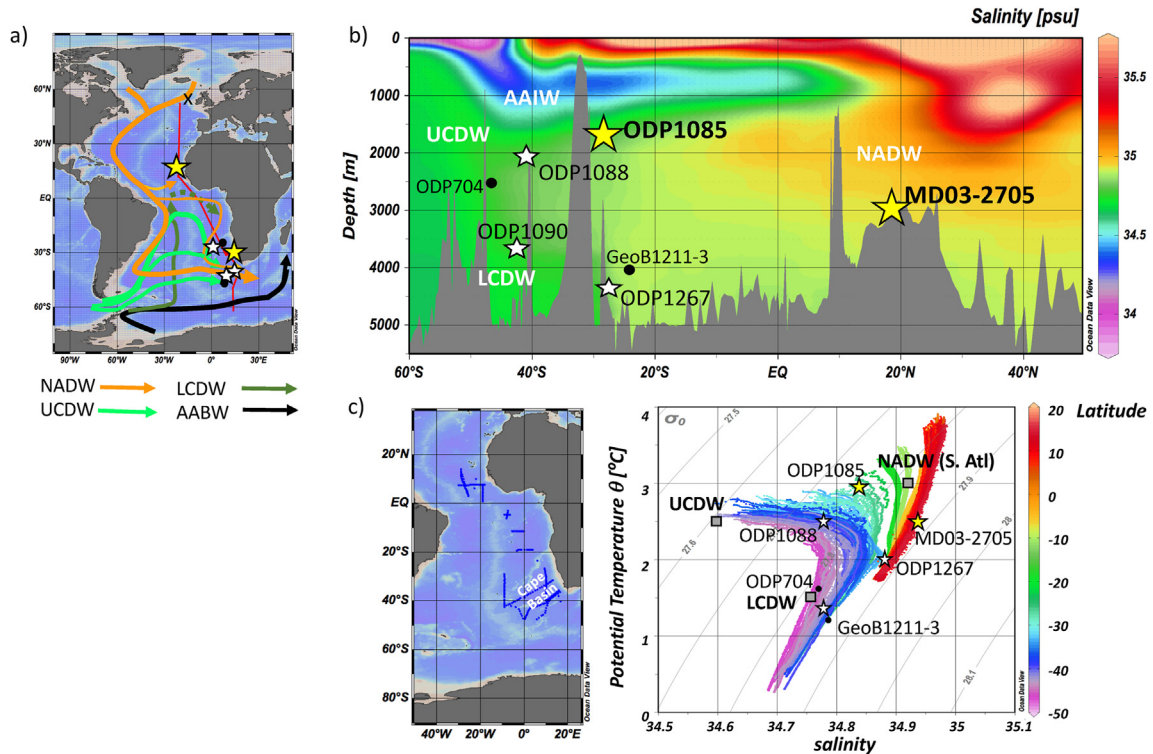
Fig. 1. Map and salinity transect showing the core locations of this study and previous studies. a) Atlantic Ocean map with the core locations of this study (yellow stars): MD03-2705 (18°06′N, 21°09′W, 3085 m) and ODP Site 1085 (29°22′S, 13°59′E, 1713 m). The white stars indicate sites where paired seawater ε_{Nd} and *C. wuellerstorfi* δ^{13}C data were reported: ODP Site 1088 (41°8.16′S, 13°33.77′E, 2082 m water depth), ODP Site 1090 (42°54.82′S, 8°53.98′E, 3702 m water depth), ODP Site 1267 (28°5.9′S, 1°42.7′E, 4355 m water depth). The black dots present the sites where strongly depleted benthic foraminiferal δ^{13}C are observed during glacial periods prior to 900 ka: GeoB1211-3 (24°29′S, 7°32′E, 4084 m water depth: Bickert and Wefer, 1996; Bickert et al., 2003), ODP Site 704 (46°53′S, 7°25′E, 2532 m water depth: Hodell and Venz, 1992). Note that site GeoB1211-3 is outside of Nambian up-welling, therefore depleted pore water δ^{13}C influence on benthic foraminiferal stable isotopes is negligible (Bickert and Wefer, 1999). The black cross shows ODP Site 982 (57°31′S, 15°52′E, 1145 m water depth: Hodell and Channell, 2016) where ice rafted material is recorded across the 900-ka event. The coloured arrows indicate flow patterns of different water masses under the modern condition. NADW = North Atlantic Deep Water, UCDW and LCDW = Upper or Lower Circumpolar Deep Water, AABW = Antarctic Bottom Water. b) Salinity transect along the red line in a) with the major water masses. Salinity data are from Antonov et al. (2010) and the symbols as for a). c) Potential temperature and salinity diagram of the present-day eastern Atlantic waters (right panel) based on Electronic Atlas of WOCE Data (https://www.ewoce.org/) at sites indicated on the left panel. The grey squares show the source water type characteristics for NADW, UCDW and LCDW (Larqué et al., 1997). Figures are visualized using the software Ocean Data View (ODV) (Schlitzer, 2015). (For interpretation of the references to colour in this figure legend, the reader is referred to the Web version of this article.)

2007). Chronostratigraphy is based on ^{14}C dating of planktonic foraminifera, benthic foraminiferal δ^{18}O tuned to the benthic LR04 stack (Lisiecki and Raymo 2005) and the paleomagnetic record (Jullien et al., 2007; Malaizé et al., 2012; Skonieczny et al., 2019). The mean sedimentation rate is 3—4 cm/kyr, and the epibenthic *C. wuellerstorfi* δ^{13}C record is available (Malaizé et al., 2012).

ODP Site 1085, drilled during Leg 175, is located in the Cape Basin in the Southeast Atlantic Ocean (Fig. 1). The site is offshore of the present-day centre of coastal Benguela upwelling, and fila-ments of cold and nutrient-rich waters can occasionally reach to the surface water overlying the core site (Wefer et al., 1998). Chronostratigraphy (Table S1) is based on correlating the benthic δ^{18}O record to the benthic LR04 stack (Lisiecki and Raymo 2005) using the shipboard biostratigraphy and magnetostratigraphy as initial tie points (Fig. S1). In this study, we focused on the first 55 m of sediments that are rich in calcium carbonate (60—85 wt%) (Wefer et al., 1998). *Cibicidoides wuellerstorfi* δ^{13}C and δ^{18}O values were determined at every 10 to 20-cm interval. Foraminiferal ε_{Nd} and U/Ca analyses were performed in the same samples covering from MIS 29 to MIS 13.

3.2. Nd isotopic composition of mixed planktonic foraminifera

Samples for ε_{Nd} analysis were selected to cover glacial and interglacial periods based on benthic foraminiferal δ^{18}O records

(Fig. S2). Details of sample preparation and Nd isotopic composition measurements are shown elsewhere (Cornuault et al., 2018; Tachikawa et al., 2014). Briefly, 20—30 mg of mixed planktonic foraminiferal tests were gently cracked to open all chambers. Clay and other fine particles were removed by repeated ultrasonication steps until the water remains were clear and free of clay. Then the test fragments were dissolved by step-wise addition of 1M acetic acid and the obtained solution was centrifuged. The obtained su-pernatants were purified by 2-step column separation using TRU.Spec and Ln.Spec resin (Pin and Santos Zalduegui, 1997). Neodymium blank of the whole procedure was better than 10 pg.

Neodymium isotopic composition was determined using a Thermo Fisher Neptune^{Plus} Multi-Collector Inductively Coupled Plasma Mass Spectrometer (MC-ICP-MS) in dry plasma mode. Typical sample size was 10—15 ng Nd and samples were introduced with an Aridus II desolvation device. ^{143}Nd/^{144}Nd was normalized to ^{146}Nd/^{144}Nd of 0.7219 using the standard exponential law. A concentration-match JNdi-1 standard solution (Tanaka et al., 2000) was analysed at every sample as a bracketing standard to monitor and correct the instrumental mass fractionation. The reported un-certainty of each sample is twice the standard error of the mea-surements. This is very close to external reproducibility (2 SD) based on the isotopic spread of the JNdi-1 standard throughout the course of the analyses: typical value of 0.2 ε-unit (Table S2a and b). The accuracy of the correction was checked by repeated

measurements of the AMES standard solution, which yields an average ε_{Nd} value of -13.0 ± 0.3 (2 SD, n = 28) agreeing well with a published value of -13.2 ± 0.3 (Chauvel and Blichert-Toft, 2001). Replicate measurements on 3 samples of core MD03-2705 present excellent agreements (Table S2a). All the analyses were carried out at CEREGE.

3.3. Planktonic foraminiferal U/Ca (ODP site 1085)

Authigenic U content was determined on planktonic foraminifer *Neogloboquadrina dutertrei* because this species was one of the most abundant in sediments at ODP Site 1085. Twenty to thirty individuals of *N. dutertrei* (250−355 μm size) per sample were weighed, gently crushed and cleaned with the "Mg method" that consists of clay removal and oxidative steps (Barker et al., 2003). Cleaned test fragments were dissolved with 0.075 M HNO_3 and centrifuged to remove any residual particles. The solutions were diluted to a Ca concentration of 100 μg/ml and analysed by ICP-MS (Agilent 7500ce) using bracketing. Analytical performance was evaluated by repeated measurements of a house standard with comparable U and Ca concentrations with foraminiferal samples at every 5 samples. Precision of U/Ca is estimated to be better than 3% and blank contribution to the foraminiferal U/Ca was negligible. The sample preparation and U/Ca analysis were realized at CEREGE.

3.4. Elemental composition and Nd isotopic ratio of fine fraction and supernatant samples (core MD03-2705)

In order to examine the cleaning efficiency to remove fine dust mineral particles attached on foraminiferal tests of core MD03-2705, chemical composition (Nd, Al, Fe, Mn, Sr and Ca) and ε_{Nd} values of fine particles were measured for selected samples: 1.8, 17.6, 403 and 439 ka, corresponding to MIS 1, 2, 11 and 12, respectively. Two ways of fine particle collection were applied to these samples. Firstly, we washed the >150 μm fraction with tap water to collect particles attached on foraminiferal tests. The obtained fine particles (<63 μm) are referred as to "fine fraction". Secondly, we recovered supernatant samples by the standard multistep ultrasonication cleaning for Nd isotopic analysis (section 3.2). The supernatant samples contain particles filled the inside of test chambers and fragmented planktonic foraminiferal tests. The collection of the supernatant was repeated 2 to 5 times (referred as supernatant, "S1 to S5") according to the presence of fine particles: S1 and S2 were collected for the MIS 1 and 2 samples, whereas more fractions were collected for MIS 11 (S1−S3) and MIS 12 (S1−S5) samples. The "fine fraction" and the particles in supernatants were dissolved by step-wise addition of 1M acetic acid to minimise the dissolution of detrital fraction. After centrifugation to remove any residual particles, the solution was evaporated and the residual was dissolved with HNO_3 for analysis by ICP-MS (Agilent 7500ce).

Since each supernatant sample did not contain enough amount of Nd for isotopic analysis, the Nd isotopic composition was determined only for the fine fraction. We focused on the samples at MIS 11 and 12 because ε_{Nd} values of foraminiferal samples at MIS 1 and 2 present an excellent agreement with those reported by a previous study (section 4.2).

3.5. Benthic foraminiferal stable isotopes (ODP site 1085)

Stable isotopic compositions ($\delta^{13}C$ and $\delta^{18}O$) of the epibenthic *C. wuellerstorfi* (250−355 μm size fraction) were measured on a Finnigan MAT 252 mass spectrometer equipped with an automated carbonate preparation line at MARUM, University Bremen. Analytical precision was 0.07‰ for $\delta^{18}O$ as referred to an internal

carbonate standard. Site 1085 sediment was sampled along the shipboard composite section every 10 cm from 0 to 19 mcd and every 20 cm from 19 to 75 mcd (Holes 1085A and B). To obtain foraminiferal stable isotope data from exactly the same depth intervals as ε_{Nd} samples, extra measurements were carried out at CEREGE using an IRMS Delta V-Plus (Thermo-Finnigan) equipped with a carbonate preparation device (Carbo-Kiel IV). The measured isotopic values were normalized against NBS19. Mean external reproducibility was better than 0.05‰ (1SD).

4. Results

4.1. Cleaning efficiency for foraminiferal tests (core MD03-2705)

Nd/Ca ratios of the fine fraction and the supernatant samples varied from below detection limit to 13 μmol/mol with generally higher values for glacial samples (Fig. 2a). The most elevated Nd/Ca was found for the fine fraction at MIS 12 of which the Al/Ca value was also the highest (25 mmol/mol, Fig. 2b). The absolute Nd/Ca value and decreasing trend differed with the samples but the values generally decreased with repeated ultrasonication steps (Fig. 2a).

Since foraminiferal Nd carriers are associated with Fe−Mn-rich phases (Tachikawa et al., 2013), Fe/Ca and Mn/Ca ratios were also examined. Typical Fe/Ca value of acid-soluble fine particles was around 8 mmol/mol but some supernatant samples (S2 at MIS 2, S3 at MIS 11, and S1-3 at MIS 12) have iron concentrations below detection limits (Fig. 2c). The most elevated Mn/Ca values were detected in the supernatants of the early steps of ultrasonication (S1-2 at MIS 2, and S2 at MIS 12), and Mn/Ca ratio gradually decreased with repeated ultrasonication steps (Fig. 2d). A similar decreasing trend was observed for Sr/Ca from around 2 mmol/mol at early to mid ultrasonication steps to 1.3−1.5 mmol/mol (Fig. 2e), typical values of planktonic foraminifera (Elderfield et al., 2000).

Neodymium isotopic composition of the fine fraction at MIS 11 is -11.4 ± 0.3, which agreed with the value of foraminiferal authigenic fraction of -11.8 ± 0.4 at the same age within uncertainty (Fig. 2f). In contrast, ε_{Nd} value of the fine fraction at MIS 12 was -10.4 ± 0.2 whereas the value of foraminiferal authigenic fraction of -11.2 ± 0.2 (Fig. 2f). Two-sample t-test yielded p-value of <0.0001, which confirms that the ε_{Nd} difference between the fine and the foraminiferal fractions is statistically significant. The fine fraction ε_{Nd} value was close to acid-soluble Saharan dust Nd isotopic composition of -10.2 ± 0.2 (Tachikawa et al., 2004).

4.2. Foraminiferal authigenic ε_{Nd} records and benthic foraminiferal $\delta^{18}O$

The foraminiferal authigenic ε_{Nd} values of MD03-2705 for the past 20 kyr agreed well with previously published values from the same area since the last deglaciation (Howe et al., 2017) (Fig. S3). Our core-top ε_{Nd} value of -12.3 ± 0.3 at 1.8 ka was slightly lower than the present-day seawater signal at proximal sites -11.8 ± 0.2 to -11.6 ± 0.2 (USGT10-07, USGT 10−09, USGT 11−22, 136−1: Stichel et al., 2015; Zieringer et al., 2019) and an expected seawater ε_{Nd} value of -11.7 calculated using an empirical equation with seawater temperature and dissolved oxygen concentration (Tachikawa et al., 2017). Two-sample t-test confirmed the significant differences. There is an increasing ε_{Nd} trend from the early to the late Holocene in the study area (Fig. S3). It is therefore possible that the observed ε_{Nd} offset between the core-top at 1.8 ka and the present-day seawater values simply reflects temporal variability of seawater isotopic composition.

For the whole study period, the foraminiferal ε_{Nd} values of MD03-2705 ranged between -12.7 ± 0.3 (MIS 13) and -10.2 ± 0.2 (MIS 16) with generally more radiogenic values during glacial
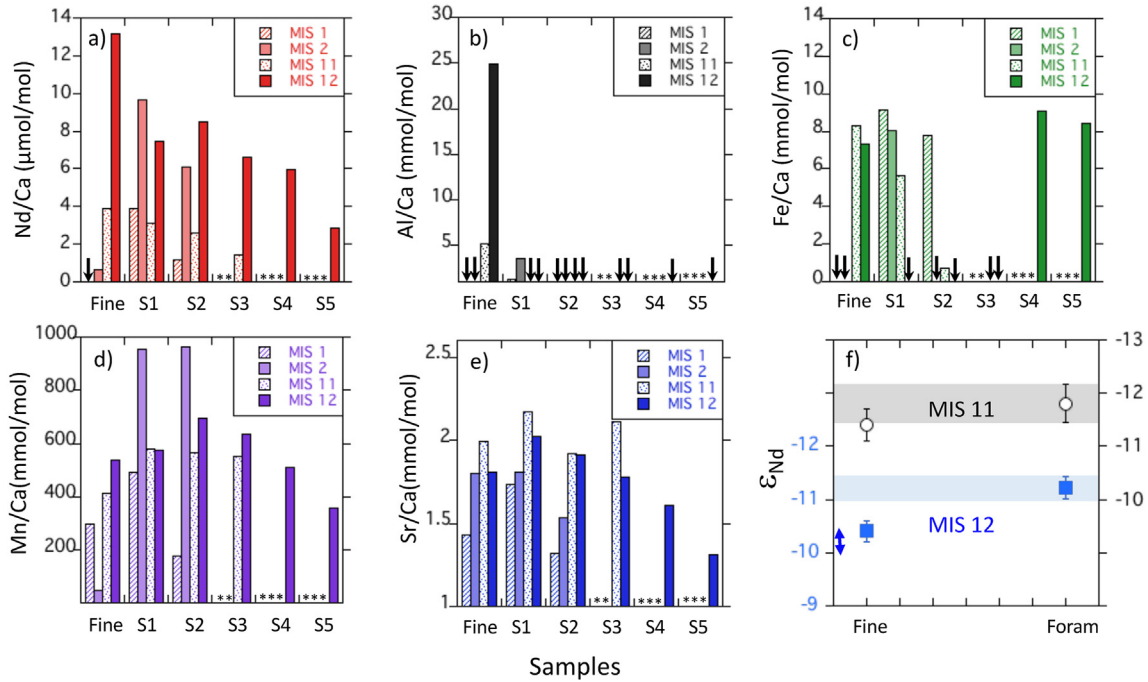
Fig. 2. Chemical composition and ε_{Nd} values of the fine particles (<63 μm) and supernatants obtained by mechanical cleaning of multi-step ultrasonication of samples at 1.8 ka (MIS 1), 17.6 ka (MIS 2), 403 ka (MIS 11) and 439 ka (MIS 12) of core MD03-2705. a) Nd/Ca, b) Al/Ca, c) Fe/Ca, d) Mn/Ca and e) Sr/Ca. The black arrows indicate samples with the elemental ratio below detection limit whereas the symbol * indicates absence of data because the collection of supernatant was not repeated. f) Comparison of ε_{Nd} values obtained for the fine particles and foraminiferal tests at MIS 11 (black) and MIS 12 (blue). The blue arrow along the y-axis indicates ε_{Nd} range of acid-soluble Saharan dust value (Tachikawa et al., 2004). (For interpretation of the references to colour in this figure legend, the reader is referred to the Web version of this article.)
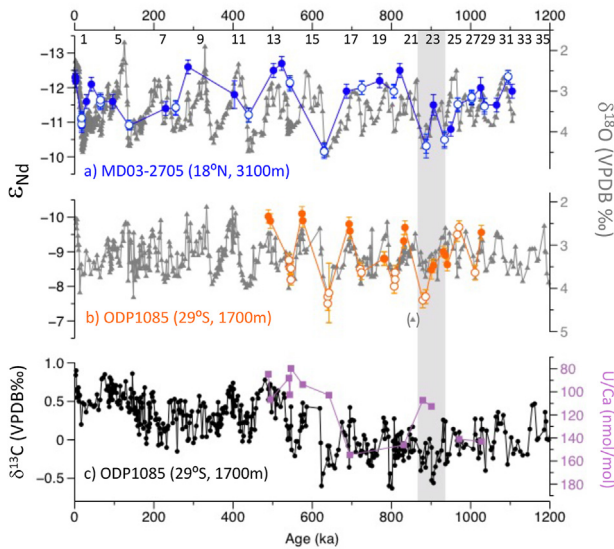

Fig. 3. Foraminiferal ε_{Nd} and *C. wuellerstorfi* $\delta^{18}O$ of MD03-2705 and ODP Site 1085 together with *C. wuellerstorfi* $\delta^{13}C$ and *N. dutertrei* U/Ca at site ODP Site 1085 over the past 1100 kyr. a) Interglacial (closed) and glacial (open) foraminiferal ε_{Nd} records and *C. wuellerstorfi* $\delta^{18}O$ (grey) of MD03–2705, b) the same as for a) in the case of ODP Site 1085, c) *C. wuellerstorfi* $\delta^{13}C$ record (black) at site ODP Site 1085 with foraminiferal U/Ca (violet). The numbers at the top correspond to MIS. The vertical grey bar represents the 900-ka event. The *C. wuellerstorfi* $\delta^{18}O$ record of core MD03-2705 is from Malaizé et al. (2012). (For interpretation of the references to colour in this figure legend, the reader is referred to the Web version of this article.)

periods (Fig. 3a and Table S2a). The most striking features of the record are low glacial ε_{Nd} values around −12 prior to the 900-ka event and an increase in ε_{Nd} values up to −10 during the 900-ka

event (Fig. 3a). Glacial/interglacial ε_{Nd} difference was very small before 900 ka. These features are consistent with the ε_{Nd} records from the Southeast Atlantic (Farmer et al., 2019; Pena and Goldstein, 2014).

The foraminiferal authigenic ε_{Nd} values at ODP Site 1085 were more radiogenic than those of core MD03-2705 (Fig. 3b, Table S2b). They ranged between −10.1 ± 0.2 (MIS 15) and −7.5 ± 0.2 (MIS 16) for the studied period (MIS 29 to MIS 13) with unradiogenic signals during interglacials. At this site, core-top and present-day seawater ε_{Nd} values are not available. The interglacial ε_{Nd} value of about −10 was higher than the present-day seawater Nd isotopic signals at 30°S to 37°S in the Southeast Atlantic of −11.0 (Stations S1 and SAVE 217: Garcia-Solsona et al., 2014; Jeandel, 1993), and the expected value of −11.6 estimated from the empirical equation (Tachikawa et al., 2017). The interglacial ε_{Nd} value is close to the modern seawater value of −10.5 to −10.0 at the closest seawater station but at 1000 m water depth (Station 40: Rahlf et al., 2020) and at 43°S to 48°S in the Southeast Atlantic (sites S2 and S3, and station 104: Garcia-Solsona et al., 2014; Stichel et al., 2012). The foraminiferal ε_{Nd} record at ODP Site 1085 shared major features identified for core MD03-2705: low glacial ε_{Nd} values prior to the 900-ka event and general increase in Nd isotopic signature at the 900-ka event (Fig. 3ab).

The $\delta^{18}O$ values of *C. wuellerstorfi* of ODP Site 1085 varied from 2.1 to 4.3‰ (values are not corrected for vital effect, Table S3) for the past 1100 kyr (Fig. 3b). The glacial-interglacial *C. wuellerstorfi* $\delta^{18}O$ amplitude is larger after 900 ka with a mean value and a standard deviation of 3.23 ± 0.34 and 3.28 ± 0.40‰ for pre- and post-900-ka event, respectively. The relative variation of the $\delta^{18}O$ record at ODP Site 1085 matched well with the LR04 reference curve (Lisiecki and Raymo, 2005) (Fig. S1).

4.3. Benthic foraminiferal δ¹³C and N. dutertrei U/Ca at ODP site 1085

Cibicidoides wuellerstorfi δ¹³C values at ODP Site 1085 showed glacial-interglacial cycles and a positive shift of mean state at around 600 ka (Fig. 3c, Table S3). From 1200 ka to 600 ka, *C. wuellerstorfi* δ¹³C values ranged between −0.6 and 0.5‰, and they varied between −0.2 and 0.9‰ after 600 ka. The lowest *C. wuellerstorfi* δ¹³C values were observed at MIS 24, 20 and 16. Between MIS 12 to 10, our *C. wuellerstorfi* δ¹³C record is in close agreement with previous δ¹³C data from Site 1085 (Dickson et al., 2008) (not shown in figure).

Since authigenic U accumulates in oxygen-depleted bottom and pore waters during post-mortem processes, foraminiferal U/Ca ratio can be used to reconstruct ocean redox chemistry (Boiteau et al., 2012). The U/Ca ratio of *N. dutertrei* at ODP Site 1085 was obtained for the same samples as for Nd isotopic measurements using a mechanical and oxidative cleaning method. The planktonic foraminiferal U/Ca values ranged between 80 and 155 nmol/mol with two mean states before and after about 600 ka as observed for the *C. wuellerstorfi* δ¹³C record (Fig. 3c, Table S2b). Higher values were found in the older part except for MIS 23 and 22, and a marked decline was observed at around 600 ka.

4.4. Relationship between ε_Nd and benthic foraminiferal stable isotopes

The foraminiferal ε_Nd and *C. wuellerstorfi* δ¹³C values of core MD03-2705 and ODP Site 1085 are broadly negatively correlated (Fig. 4). The core-top value of core MD03-2705 was on the binary mixing envelope defined by present-day NADW and CDW properties (Key et al., 2004; Schmittner et al., 2013; Tachikawa et al., 2017). The majority of data points fall below the mixing envelope, and this means lower δ¹³C than predicted by the mixing relationship. At ODP Site 1085, *C. wuellerstorfi* δ¹³C values after 600 ka (MIS 13 to 15) were less depleted than for the older part, and they are located nearby the mixing curve (Fig. 4a).

For core MD03-2705, the interglacial data points (lower *C. wuellerstorfi* δ¹⁸O values) are plotted closer to the mixing envelope than the glacial data (Fig. 4b). Such a trend is not clearly observed for the data of ODP Site 1085.

5. Discussion

The cleaning experiments for core MD03-2705 show the decreasing Nd/Ca, Al/Ca, Mn/Ca and Sr/Ca values of acid-soluble fine particles with repeated ultrasonication steps (Fig. 2). The Nd/Ca and Al/Ca ratios are generally higher for glacial samples (Fig. 2a and b), and ε_Nd values of the fine fraction and cleaned foraminiferal tests are slightly different at MIS 12 (Fig. 2f). Knowing that dust contents at site MD03-2705 were generally higher during glacial conditions (Jullien et al., 2007; Tisserand et al., 2009; Malaizé et al., 2012; Skonieczny et al., 2019), these results suggest that the glacial fine particles may contain more acid-soluble detrital carbonates derived from Saharan dust. The mechanical cleaning is effective to remove the detrital carbonates since the chemical composition of supernatant samples approached towards that of foraminiferal tests with multi-step ultrasonication as shown by Sr/Ca ratios (Fig. 2e).

We are confident that the MD03-2705 foraminiferal ε_Nd values represent bottom/pore water signals that are not affected by Saharan dust inputs due to insufficient cleaning based on following evidences: (i) common features of ε_Nd records of cores MD03-2705 and ODP Site 1085, the latter of which is free from Saharan dust influence (Fig. 3a and b); (ii) close match of the MD03-2705 ε_Nd values with the previous results from the same area during the Holocene and the LGM (Howe et al., 2018) independently obtained by a distinct number of fine particle removal steps (Fig. S3); and (iii) ultrasonication steps repeated more than five times until achievement of transparent supernatants. The influence of reactive detrital phases on foraminiferal ε_Nd values via Nd in pore water is a matter of debate and cannot be totally ruled out.

At ODP Site 1085, *C. wuellerstorfi* δ¹³C was lower and foraminiferal U/Ca was higher at the 1200−600 ka interval than for the
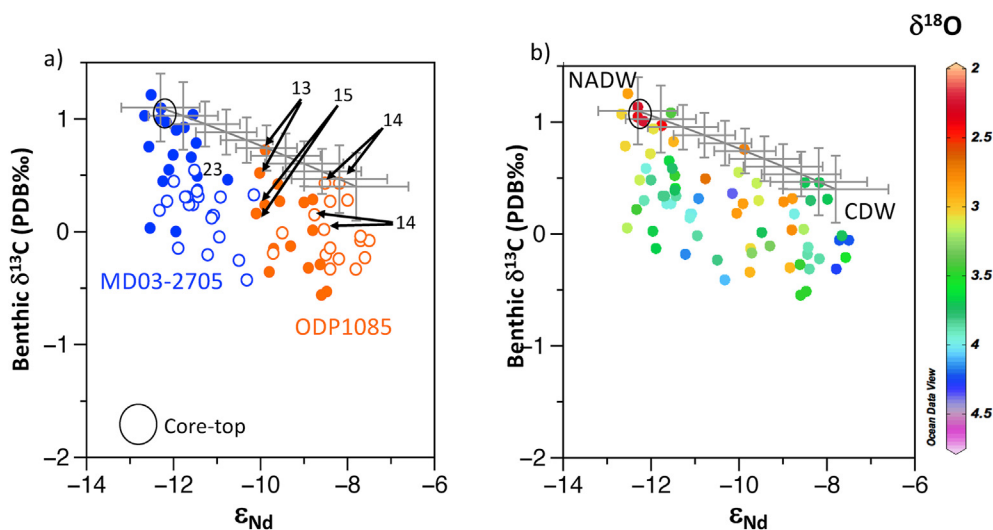

Fig. 4. Relationship between foraminiferal ε_Nd and *C. wuellerstorfi* δ¹³C. a) The relationship of cores MD03-2705 (blue) and ODP Site 1085 (orange). The arrows and numbers indicate ODP Site 1085 samples after 600 ka and corresponding MIS. b) The same relationship with *C. wuellerstorfi* δ¹⁸O values with colour code. A binary mixing line (the grey curves in a and b) is defined by the present-day NADW and CDW endmembers: for NADW, ε_Nd = −12.3 ± 0.9 (1σ), dissolved Nd concentration = 20.3 ± 3.2 (1σ) pmol/kg, δ¹³C-DIC = 1.1 ± 0.3‰ (uncertainty is arbitrarily fixed to be 0.3‰) and DIC concentration = 2175 ± 109 μmol/kg (uncertainty is arbitrarily fixed to be 5%). For CDW, ε_Nd = −7.8 ± 1.2 (1σ), dissolved Nd concentration = 24.0 ± 4.8 (1σ) pmol/kg, δ¹³C-DIC = 0.4 ± 0.3‰ (uncertainty is arbitrarily fixed to be 0.3‰), DIC concentration = 2285 ± 114 μmol/kg (uncertainty is arbitrarily fixed to be 5%). The ε_Nd values and Nd concentration are based on Tachikawa et al. (2017) whereas the δ¹³C-DIC and the DIC concentration values are from Schmittner et al. (2013) and Key et al. (2004), respectively. (For interpretation of the references to colour in this figure legend, the reader is referred to the Web version of this article.)

last 600 ka interval (Fig. 3c). These features can be interpreted as a sign of more corrosive and reducing environment for the older part in relation to the past upwelling activity (Dickson et al., 2010; Wefer et al., 1998). The Benguela upwelling system has evolved under the influence of combined effects of major global wind and oceanic systems as well as local variations in the strength and/or position of the winds (Petrick et al., 2018). There was a series of key periods of the system evolution since the last 1.5 Ma. One of them is the time interval around 600 ka that corresponds to a northward shift of the Benguela current cells (Petrick et al., 2018). Therefore the δ^{13}C record at ODP Site 1085 will be interpreted with caution, although the influence of productivity changes on the δ^{13}C values may be of secondary importance considering continuous occurrence of the oxic and oligotrophic benthic species *C. wuellerstorfi* (Jorissen et al., 2007).

5.1. AMOC changes at the 900-ka event

In order to examine spatiotemporal tendency of seawater ε_{Nd} across the MPT, all the available reconstructed seawater ε_{Nd} records covering the 900-ka event are compared: MD03-2705 and ODP Site 1085 (this study), ODP Site 1088 (Dausmann et al., 2017; Hu et al., 2016; Pena and Goldstein, 2014), ODP Site 1090/TTNO57-6 (referred as to ODP Site 1090) (Howe et al., 2016; Pena and Goldstein, 2014) and ODP Site 1267 (Farmer et al., 2019) (Figs. 1 and 5b). ODP Site 1267 is in the Angola Basin, north of Walvis Ridge in the Southeast Atlantic at a water depth of 4400 m where this bathymetric barrier minimizes the influence of SSW (Farmer et al., 2019) and NADW is estimated to be the major water mass (Fig. 1c).

The remarkable feature of the ε_{Nd} records is a persistent meridional seawater Nd isotopic gradient for the past 1100 kyr (Fig. 5b), being consistent with previous studies (e.g., Goldstein et al., 2017). The Nd isotopic composition is systematically lower at MD03-2705 and ODP Site 1267 where NADW is currently the major water mass than at ODP Site 1085, ODP Site 1088 and ODP Site 1090 in the South Cape Basin, influenced by a greater proportion of SSW such as UCDW, LCDW and AABW at the present day (Rahlf et al., 2020) (Figs. 1 and 5b). These three sites (ODP Sites 1085, 1088 and 1090) present similar ε_{Nd} values and relative variability (Fig. 5b). All the records indicate lower glacial ε_{Nd} values before 900 ka than for more recent glacial periods, and an increase in seawater Nd isotopic composition during the 900-ka event.

These basin-wide features could be explained by changes in NSW and SSW productions. However, variation of the NSW/SSW ratio alone does not allow determining whether changes are derived from the northern or southern hemisphere. To obtain insight into possible mechanisms responsible for the positive ε_{Nd} shift at the 900-ka event, reconstructed seawater ε_{Nd} distribution is compared with modelling results. A previous study simulated global seawater ε_{Nd} values with Earth system Models of Intermediate Complexity (EMIC) assuming that the boundary exchange (particle-dissolved exchange of Nd isotopes around continental margins) was the only Nd source to the ocean (Friedrich et al., 2014). Reduction of the AMOC was realized by excess freshwater inputs to the North Atlantic whereas Southern Ocean Meridional Overturning Circulation (SOMOC) was amplified by removal of freshwater from the Southern Ocean (Friedrich et al., 2014).

A general increase in seawater ε_{Nd} values was simulated in the case of reduced AMOC (Friedrich et al., 2014), which is consistent with the reconstructed seawater ε_{Nd} distribution in the Atlantic. In contrast, the increased SOMOC has little influence on the Atlantic seawater ε_{Nd} values (Friedrich et al., 2014). Similar results were obtained using an independent EMIC that considered both dissolved Nd concentration and Nd isotopic composition (Rempfer

et al., 2012). These results suggest that the basin-wide seawater ε_{Nd} increase at the 900-ka event can be better explained by reduced AMOC (Tachikawa et al., 2020).

5.2. Impact of changes in Nd sources to the North Atlantic on seawater ε_{Nd} distribution

Another possibility to modify large-scale seawater ε_{Nd} distribution is changes in Nd sources to the North Atlantic in relation to modified dissolved-particulate interaction that was produced by shift of convection zone and/or water flow pathway. Several modelling studies (Arsouze et al., 2008; Menviel et al., 2020) and reconstructions (Gutjahr et al., 2008; Zhao et al., 2019; Du et al., 2020; Pöppelmeier et al., 2020) pointed out possible changes in ε_{Nd} value of the NSW endmember on glacial/interglacial scale. During the Last Glacial Maximum (LGM), reduced Nd contribution from Baffin Bay with very low ε_{Nd} to the NADW formation zone, and southward migration of convection zone due to sea ice extension towards the Norwegian Sea could have increased the Nd isotopic signature of NSW (Du et al., 2020; Menviel et al., 2020). Fundamental changes in the Northern cryosphere occurred across the MPT (Clark et al., 2006) with the first sea level drop at MIS 22 that was estimated with bottom water δ^{18}O reconstruction (Elderfield et al., 2012) although it is still debated whether the observed δ^{18}O signal is a global sea level signal (Ford et al., 2016). Even if the past convection zone and sea ice extension in the North Atlantic over the MPT have not been determined yet, the inception of conditions similar to those of peak glaciations in the 100 kyr world could have occurred across the MPT. The condition could modify Nd sources to the ocean.

To evaluate the potential impact of changes in Nd sources to the North Atlantic on seawater ε_{Nd} distribution, we use a PANDORA 10-box model (Fig. S4) (Tachikawa et al., 2003) that is calibrated with an updated compilation of global seawater Nd concentration and isotopic composition (Tachikawa et al., 2017). External Nd sources to North Atlantic, surface Atlantic, North Pacific and surface INDOPAC (Indian-Pacific Oceans) boxes, and ε_{Nd} values of these sources are determined using the compiled data (Table S4). Oceanic Nd residence time is fixed to be 700 yr (Rempfer et al., 2012). The scavenged Nd flux from each box is calculated at steady state to balance advective Nd fluxes between different boxes. Then, the scavenging coefficient is determined for perturbation experiments, by dividing scavenged Nd flux by dissolved Nd concentration (Table S4). The scavenging coefficient of each box is assumed to be constant with time.

We examine the influence of more radiogenic Nd source to the North Atlantic box under three circulation states: present circulation (Broecker and Peng, 1987), reduced AMOC (10 Sv, Sverdrups = 10^6 m^3/s, instead of 20 Sv) and increased SOMOC (+4 Sv to the deep Atlantic and to the deep INDOPAC; Fig. S4). Water fluxes were adjusted to maintain water volume of each box. The ε_{Nd} value of the external source to the North Atlantic is increased by adding +2, +4 and + 6 ε-units to the initial value (Table S4). For comparison, circulation change experiments are conducted without any modification of Nd isotopic signature of the source ("No change" experiment). We neither intend to precisely reproduce the seawater ε_{Nd} distribution at the 900-ka event nor examine the possible shoaling of the AMOC. These are sensitivity tests to evaluate how the modified Nd supply to the North Atlantic box propagates and affects seawater ε_{Nd} distribution under different circulation conditions.

The result of reduced AMOC "No change" experiment shows a marked ε_{Nd} decrease in the North Atlantic, little ε_{Nd} change in the deep Atlantic, and a clear positive isotopic shift in the deep

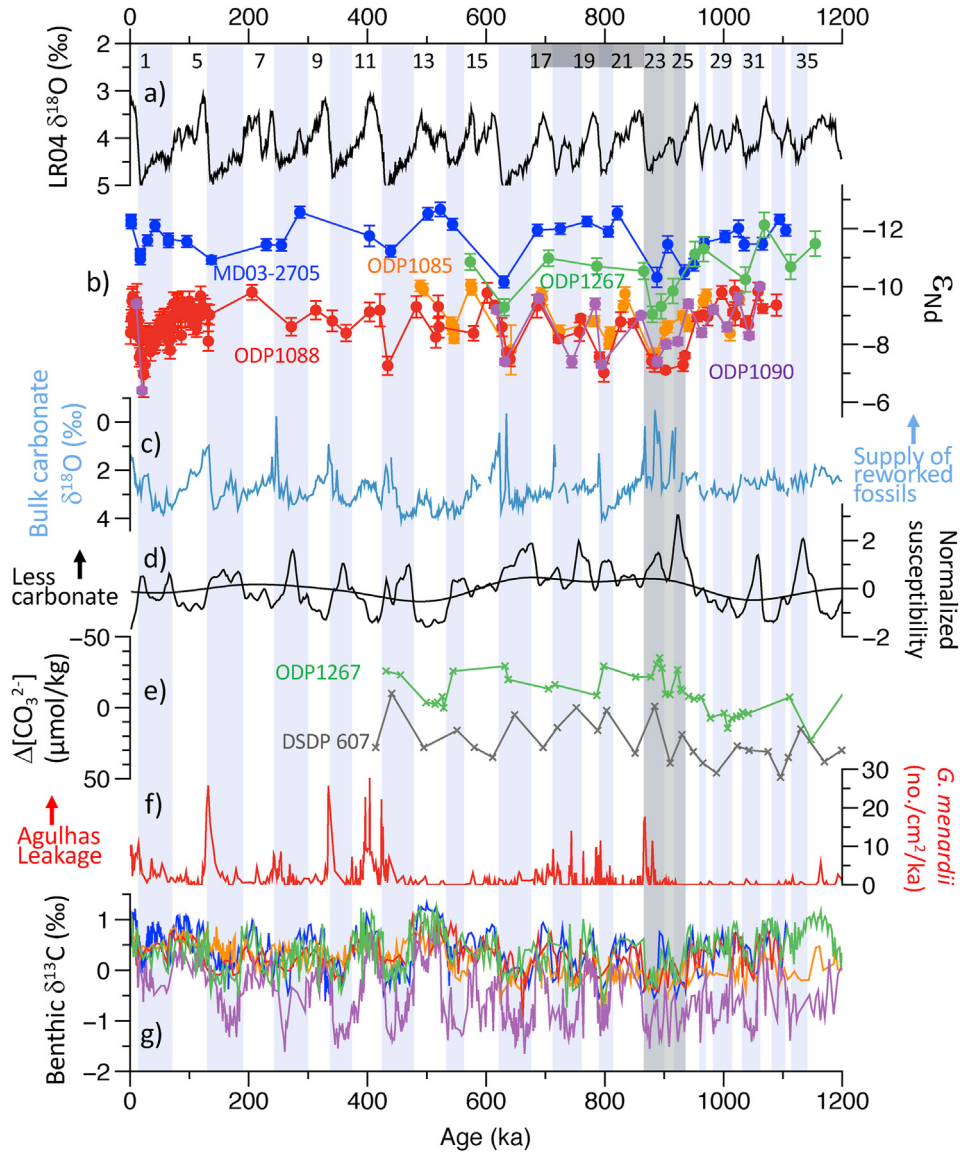**Fig. 5.** Foraminiferal ε_{Nd} and *C. wuellerstorfi* $\delta^{13}C$ time series from the eastern Atlantic over the past 1100 kyr compared with other records. a) Stacked benthic foraminiferal $\delta^{18}O$ record LR04 (Lisiecki and Raymo, 2005). b) Foraminiferal ε_{Nd} records of MD03-2705 (blue, this study) and ODP Site 1085 (orange, this study), ODP Site 1267 (green) (Farmer et al., 2019), ODP Site 1088 (red) (Dausmann et al., 2017; Hu et al., 2016; Pena and Goldstein, 2014), and ODP Site 1090/TTNO57-6 (violet) (Howe et al., 2016; Pena and Goldstein, 2014). c) Bulk carbonate $\delta^{18}O$ at site ODP Site 982 as an indicator of reworked nannofossil supply associated with Eurasian Ice Sheet evolution (Hodell and Channell, 2016). d) Stacked calcium carbonate content in bulk sediments at around 25 to 35°S in the Atlantic Ocean deduced from magnetic susceptibility. The smoothed curve shows a long-term trend (low-pass filtering > 350 kyr) (Schmieder et al., 2000). e) *C. wuellerstorfi* B/Ca derived $\Delta[CO_3^{2-}]$ reconstruction at DSDP Site 607 (41°N, 33°W, 3427 m water depth) in the North Atlantic (Lear et al., 2016) and at ODP Site 1267 (Farmer et al., 2019). f) *Globorotalia menardii* accumulation rate at ODP Site 1087 (31°28′S, 15°19′E, 1371 m water depth) as an indicator of Agulhas leakage (Caley et al., 2012). g) *C. wuellerstorfi* $\delta^{13}C$ time series of the five cores. Colour code is the same as for b). The light grey bar and blue bars indicate the 900-ka event and glacial periods, respectively. The dark grey rectangle shows the MPT interim period (920–640 ka). (For interpretation of the references to colour in this figure legend, the reader is referred to the Web version of this article.)

Southern Ocean ("deep Antarctic") and INDOPAC (Fig. 6a). The weaker NADW production allows the accumulation of unradiogenic Nd in the North Atlantic whereas the reduced advection of unradiogenic Nd results in the positive ε_{Nd} shift in the deep Southern Ocean and INDOPAC. The Nd advection from the North Atlantic with the lowest ε_{Nd} value and that from the other oceans with higher ε_{Nd} values to the deep Atlantic leads to a small isotopic change. The enhanced SOMOC "No change" experiment yields a slight positive (negative) shift in the deep Atlantic (deep INDOPAC) because the Southern Ocean ε_{Nd} value is intermediate between the deep Atlantic and INDOPAC values (Fig. 6b). This SOMOC + result is comparable with and EMIC results (Rempfer et al., 2012; Friedrich

et al., 2014) whereas the reduced AMOC "No change" is clearly different between the two types of models. The difference can be explained by the fact that changes in Nd sources to the oceans are integrated in EMIC simulations as the boundary exchange (Rempfer et al., 2012; Friedrich et al., 2014). The effect of boundary exchange is stronger in the North Atlantic surrounded by continents with contrasted ε_{Nd} values (Jeandel et al., 2007) than in the Southern Ocean.

All the box model simulation results demonstrate that the radiogenic Nd perturbations to the North Atlantic are propagated on global scale, with a more radiogenic Nd source to the North Atlantic leading to more positive seawater Nd isotopic shifts
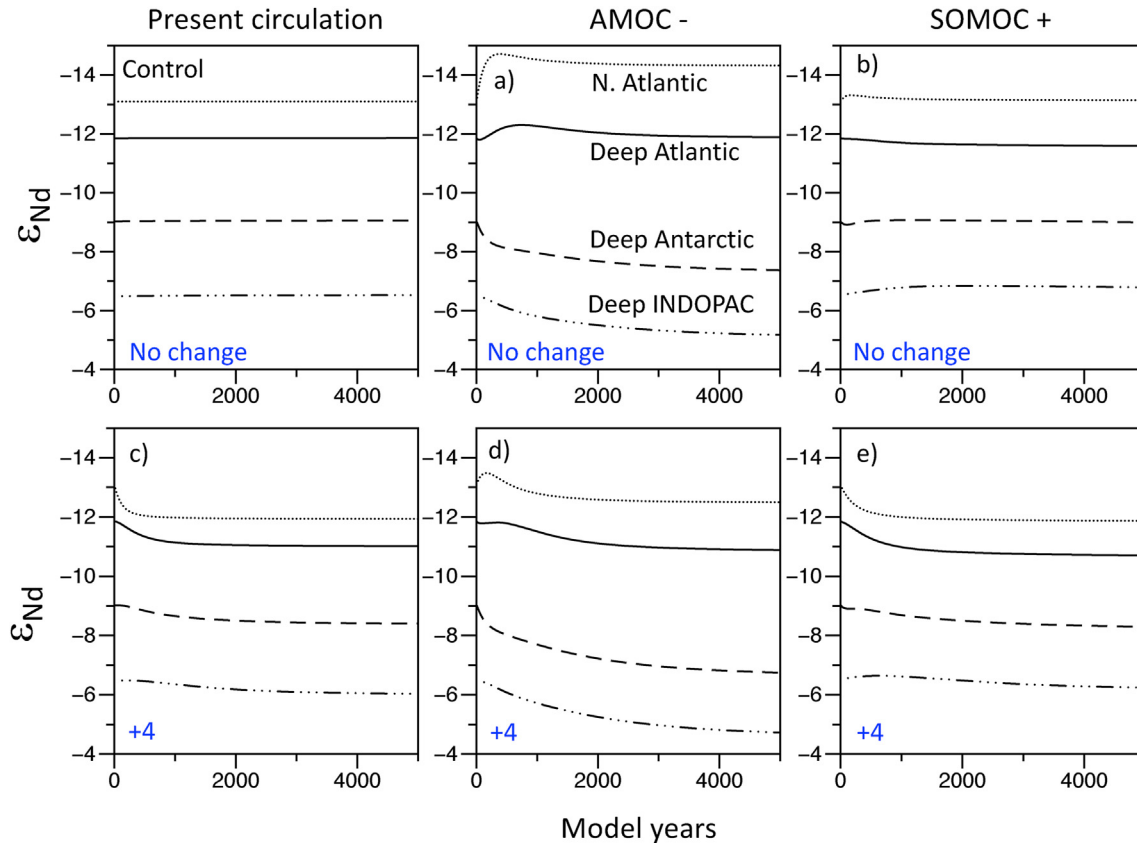
Fig. 6. Sensitivity tests of seawater ε_{Nd} as a function of model years using PANDORA 10-box model. Simulated values are indicated for North Atlantic, deep Atlantic, deep Antarctic and deep INDOPAC (deep > 1000 m). The ε_{Nd} value of external source to the North Atlantic is increased by adding +2, +4 and + 6 ε-units to the initial value (Table S4). The upper three panels (control, a and b) indicate the seawater ε_{Nd} variability without any change of Nd external source ('No change') whereas the lower three panels (c, d, and e) show the cases with +4 ε-unit addition. The results of +2 and + 6 ε-unit addition are shown in Fig. S5. See text for details about AMOC- and SOMOC+.

(Fig. 6c, d and e and S5). For instance, the Nd sources with an increase of +2, +4 and + 6 ε-units yield the ε_{Nd} shifts of +0.4, +1.0 and + 1.5 in the deep Atlantic under the reduced AMOC condition, respectively (Figs. 6d and S5). The global positive ε_{Nd} shift is the most pronounced in the reduced AMOC experiment (Fig. 6d) because of the smaller NADW advection that transports low ε_{Nd} seawater to the other oceanic regions.

Proxy reconstructions demonstrate that the positive ε_{Nd} shift at the 900-ka event is not limited to the Atlantic Ocean. Positive ε_{Nd} events at 900-ka are observed at ODP Site 748 in the North Indian Ocean (Williams, 2018) and ODP Site 1234 in the Southwest Pacific (Piotrowski et al., 2015). The result of the enhanced SOMOC "No change" experiment is not compatible with this global feature (Fig. 6b). Even though a generally positive ε_{Nd} shift can be produced with radiogenic Nd sources under the enhanced SOMOC or the present-day circulation (Figs. 6c, e and S5), we assume that such cases are difficult to realise because processes affecting the external Nd sources to the North Atlantic could modify the hydrological cycle of the surface Atlantic, thus AMOC strength (see section 5.4). In the following, we examine the hypothesis that more radiogenic Nd sources and a weaker AMOC were the main cause of the positive ε_{Nd} shift at the 900-ka event rather than a stronger SOMOC.

5.3. $\delta^{13}C$ and ε_{Nd} relationship in the eastern Atlantic Ocean

The hypothesis can be examined using the relationships between foraminiferal ε_{Nd} and benthic foraminiferal $\delta^{13}C$. In the modern Atlantic, a binary mixing between NADW and CDW

explains the relationship between seawater ε_{Nd} and $\delta^{13}C$ value of dissolved inorganic carbon (δ^{13}C-DIC) at water depths deeper than 1500 m (Fig. 7). If the Nd supply to the North Atlantic becomes more radiogenic, the ε_{Nd} value of both NSW and SSW increases, as shown by the global positive isotopic shifts (Fig. 6 and S5). The new binary mixing curve would be formed above the initial one with a general shift towards higher ε_{Nd} values (Fig. 7a: the black triangles, circles and diamonds indicate the binary mixing trends when the Nd sources to the North Atlantic are more radiogenic with an increase of +2, +4 and + 6 ε-units, respectively). If the δ^{13}C-DIC values of NSW and SSW decrease because of accumulation of remineralised organic matter in relation to slow ventilation and/or restricted air-sea exchange (Mix and Fairbanks, 1985; Gebbie, 2014), a new mixing curve would be formed below the initial one (Fig. 7a). These features are used to evaluate the above-mentioned hypothesis.

Before comparing the past ε_{Nd} - $\delta^{13}C$ relationship with the present-day binary mixing, benthic $\delta^{13}C$ records are corrected for a long-term global ocean $\delta^{13}C$ change provided by Hoogakker et al. (2006) (Fig. S6). Stacked *C. wuellerstorfi* $\delta^{13}C$ record reflects the global modification of terrestrial carbon storage on the glacial/interglacial timescale and changes in the burial fluxes of organic and inorganic carbon on longer time scales (Hoogakker et al., 2006). We compare *C. wuellerstorfi* $\delta^{13}C$ records (Fig. 5g) between ODP Site 1085 (this study), MD03-2705 (Malaizé et al., 2012), ODP Site 1267 (Bell et al., 2014), ODP Site 1088 and ODP Site 1090 (Hodell et al., 2003a) and subtract the stacked $\delta^{13}C$ from each *C. wuellerstorfi* $\delta^{13}C$ record (Fig. S6). The obtained records are
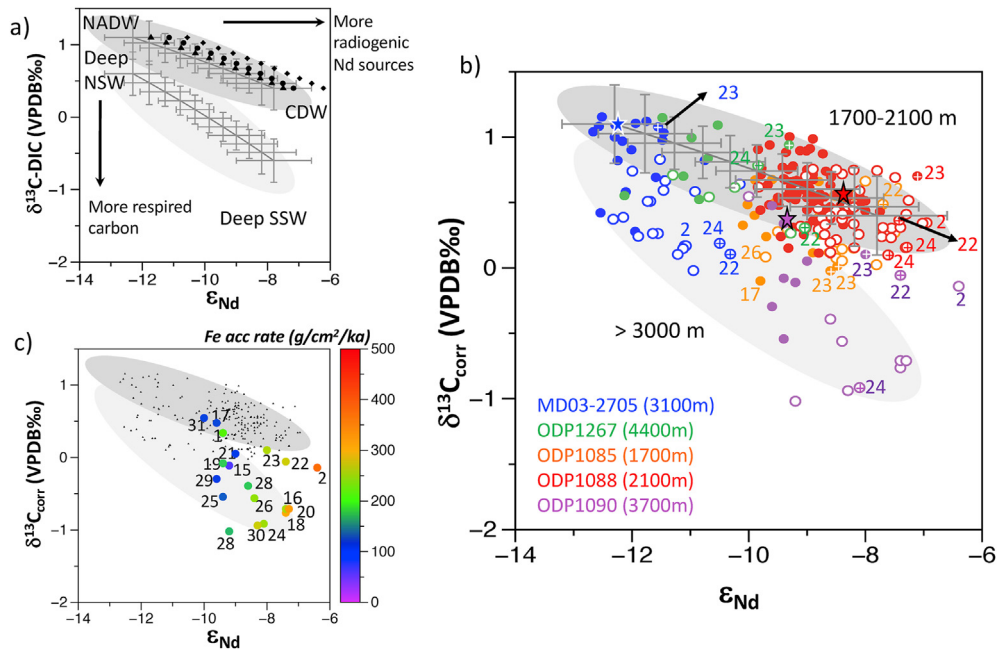
Fig. 7. Relationship between $\delta^{13}C$ and ε_{Nd}. a) The binary mixing curve formed by the present-day NADW and CDW endmembers is the upper grey line. The definition of each endmember is in Fig. 4 caption. The black triangles, circles and diamonds indicate the binary mixing trend when the Nd sources to the North Atlantic are more radiogenic with an increase of +2, +4 and +6 ε-units, respectively. The lower grey line with "Deep NSW" and "Deep SSW" shows an example of mixing with endmembers characterised by more respired carbon: the $\delta^{13}C$-DIC values of NADW and CDW are decreased by subtracting of 0.5 and 1.0‰ from the initial values, respectively. The light and dark grey ellipses approximately cover data points from the intermediate and deep water depths shown in b), respectively. b) Relationship between *C. wuellerstorfi* $\delta^{13}C$ corrected for global changes in the carbon cycle ($\delta^{13}C_{corr}$, see text for more detail) and foraminiferal ε_{Nd} of cores MD03-2705, ODP Site 1085, ODP Site 1088, ODP Site 1090 and ODP Site 1267. The closed and open symbols indicate interglacial and glacial data points, respectively. The cross symbols show data from MIS 24–22. The coloured stars show core-top values at different sites. The numbers indicate MIS. c) Relationship between $\delta^{13}C_{corr}$ and ε_{Nd} with iron accumulation rate of ODP Site 1090 (Martinez-Garcia et al., 2011) with the colour code. The iron accumulation rate is integrated for 10 kyr considering that $\delta^{13}C$ data represent a time-average response to local productivity. The numbers indicate MIS. The small black dots indicate the data points shown in b). (For interpretation of the references to colour in this figure legend, the reader is referred to the Web version of this article.)

referred as corrected $\delta^{13}C$, $\delta^{13}C_{corr}$. The $\delta^{13}C_{corr}$ values reflect the local/regional variation of biological productivity, the ventilation rate and the air-sea exchange of CO_2 in the surface ocean regions of NSW and SSW formation. Some data of ODP Site 1085 such as at MIS 17 and 26 are characterised by lower $\delta^{13}C_{corr}$ than expected values from the binary mixing (Fig. 7b). They can be explained by the fluctuation of local biological productivity as shown by lower benthic $\delta^{13}C$ values and higher U/Ca for 1200–600 ka interval including MIS 17 and 26 than for 0–600 ka interval (Fig. 3c).

The relationship between foraminiferal ε_{Nd} and $\delta^{13}C_{corr}$ of the five cores reveals a clear trend with water depths (Fig. 7b). The majority of data from intermediate water depths (1700–2100 m) are on the present-day binary mixing envelope whereas the data from North Atlantic glacial deep water (>3000 m, MD03-2705) and South Atlantic deep waters (ODP Site 1090) at MIS 31 to 15 present lower $\delta^{13}C_{corr}$ than the present-day binary mixing envelope between NADW and CDW. Some scatters and offsets from the mixing envelope can be explained by chronological uncertainty of each record to calculate $\delta^{13}C_{corr}$ (Fig. S6). The data points at the 900-ka event (MIS 24–22, Fig. 7b) do not systematically fall above the present-day mixing curve, suggesting that the more radiogenic Nd supply could be accompanied by the accumulation of respired carbon. The 900-ka event is one of the extreme cases of reduced $\delta^{13}C_{corr}$ of deep waters as shown by large offsets from the mixing envelope at MIS 22 and 24 of core MD03-2705 and MIS 24 at ODP Site 1090 (Fig. 7b). The marked accumulation of respired carbon in the deep South Atlantic is difficult to reconcile with more active SOMOC. At MIS 23, all data points at the five sites approximately fall on the present-day mixing envelope whatever the water depths with high ε_{Nd} values (Fig. 7b). Since the stacked $\delta^{13}C$ shows the

lowest $\delta^{13}C$ at MIS 23 over the past 1200 kyr (Fig. S6), we interpret this result as the accumulation of respired carbon in the global ocean. These observations support the idea that more radiogenic Nd supply combined with the reduced AMOC was the main cause of the positive ε_{Nd} shift at the 900-ka event rather than stronger SOMOC.

Both proxy reconstruction and modelling study suggest that one of the possibilities to lower $\delta^{13}C$-DIC in the Southern Ocean is an increase in biological productivity via iron fertilisation (Jaccard et al., 2013; Muglia et al., 2018). To evaluate the impact of iron fertilization, the relationship between $\delta^{13}C_{corr}$-ε_{Nd} and iron accumulation rate at ODP Site 1090 is examined (Martinez-Garcia et al., 2011) (Fig. 7c). At MIS 18 and 20, $\delta^{13}C_{corr}$ values at ODP Site 1090 are strongly negative with high iron accumulation rate, being consistent with the iron fertilization hypothesis. However, depleted $\delta^{13}C_{corr}$ data are also observed with low iron accumulation rate such as at MIS 28 and 24 (Fig. 7c). This suggests that iron supply, promoting higher productivity, is not the only factor to reduce $\delta^{13}C_{corr}$ values.

In the next section, we discuss possible processes for the changes in Nd sources, the reduction of AMOC and the accumulation of respired carbon in the deep Atlantic for the whole study period.

5.4. Possible processes and carbon storage in the deep Atlantic Ocean

The glacial ε_{Nd} values from 1100 kyr to the 900-ka event are lower than the more recent glacial values at the five sites (Fig. 5b). This suggests dominant NSW contribution (and/or more

unradiogenic Nd supply to the North Atlantic) even at the glacial periods. However, benthic $\delta^{13}C$ values at ODP Site 1090 during this time interval are generally low (Fig. 5g), indicating the presence of poorly ventilated deep water. The presence of poorly ventilated water is also suggested by low epibenthic $\delta^{13}C$ values at ODP Site 704 (47°S, Hodell and Venz, 1992) and site GeoB1211-3 at 4100 m water depth on the southern side of Walvis Ridge (Bickert and Wefer, 1996; Bickert et al., 2003) (Fig. 1). These results contrast well with high $\delta^{13}C$ values at ODP Site 1267 on the northern side of Walvis Ridge (Figs. 1, 5f and 7b) where AABW inflow from the south is prevented due to the bathymetric barrier. Taken together, the records demonstrate even under the active AMOC condition, ventilation of deep SSW in the Southeast Atlantic was limited during the interval from 1100 kyr to the 900-ka event.

At MIS 24 to 22, the first decrease in bulk carbonate $\delta^{18}O$ occurred at ODP Site 982 on the Rockall Plateau in the Northeast Atlantic (Fig. 5c), and the negative $\delta^{18}O$ peaks are concomitant with high magnetic susceptibility (Hodell and Channell, 2016). The $\delta^{18}O$ value close to zero indicates that the source of carbonates are reworked nannofossils supplied from the Norwegian shelf and/or the northern North Sea/Denmark area to the Rockall Plateau (Hodell and Channell, 2016; Marino et al., 2011). This result may suggest an expansion of Eurasian Ice sheet and possible seasonal instability of the ice sheet during the 900-ka event. Because of the proximal position to source areas of deep-water formation, the Eurasian ice sheet might have had strong impact on deep-water formation in spite of its small influence on global ice volume (Hodell and Channell, 2016). We note here that the Norwegian shelf and/or the northern North Sea/Denmark area are characterised by higher ϵ_{Nd} values than areas of the Northern northwest Atlantic coast such as the Greenland shelf and Baffin Bay (Jeandell et al., 2007). Considering these points, we propose a hydrological perturbation originating from the Eurasian Ice Sheet which induced the changes in Nd supply to the North Atlantic. It is worth noting that the AMOC was less stable than previously thought over the past 500 kyr, and a small perturbation of the hydrological cycle could trigger reduced NADW production (Galaasen et al., 2020).

After the 900-ka event, foraminiferal ϵ_{Nd} values at interglacial periods were as low as the present bottom water values (Fig. 5b), indicating reactivation of the AMOC (Pena and Goldstein, 2014). The more active AMOC could be related with global reorganization of thermohaline circulation. For instance, significantly intense Agulhas leakage events were reconstructed after the MIS 22/21 transition (Caley et al., 2012) (Fig. 5f) and extra salt supply from the southern hemisphere to the North Atlantic could have contributed to stronger interglacial AMOC (Biastoch et al., 2008; Knorr and Lohmann, 2003).

Glacial deep Atlantic waters after the 900-ka event are characterised by $\delta^{13}C_{corr}$ values lower than the expected from the mixing envelope, similar to MIS 24 and 22 (Fig. 7b). Since the $\delta^{13}C_{corr}$ depletion is observed for both North (MD03-2705) and South Atlantic (ODP Site 1090), we infer weaker production and shallower flow of NSW as well as stagnant ventilation and/or restricted air/sea exchange of deep SSW relative to the interglacial periods. This inference is consistent with the following reconstructions. From MIS 22 to MIS 16, a gradual reduction of glacial AABW formation was estimated based on enhanced stratification in the Southern Ocean in relation to the growth of fresh water cap (Hasenfratz et al., 2019). The strong stratification prevented active AABW formation, leading to corrosive deep waters. The presence of corrosive waters is also suggested by calcium carbonate contents in bulk sediments. The period from MIS 22 to MIS 16 corresponds to the interval called "a MPT interim" (920–640 ka; Schmieder et al., 2000) that is characterised by low calcium carbonate content in bulk sediments, in particular during glacial periods at around 25 to 35°S at water depth 2900–4500 m in the South Atlantic as shown by the SUSAS stack (Fig. 5d). The carbonate content varied at ODP Site 1090 at 3702 m water depth (21–92% of carbonate in bulk sediments) in a similar way to SUSAS stack. It is interesting to note that almost constant and systematically higher carbonate content (78–95%) is found at ODP Site 1088 at 2082 m water depth (Hodell et al., 2003b). The better carbonate preservation at intermediate water depths is consistent with the two mixing envelopes based on the $\delta^{13}C_{corr}$ - ϵ_{Nd} relationship (Fig. 7b) and our hypothesis of more corrosive water at deeper water depths.

It is interesting to note that the existence of corrosive glacial deep waters since the 900-ka event was proposed based on *C. wuellerstorfi* B/Ca derived $\Delta[CO_3^{2-}]$ reconstructions in the North and South Atlantic (Fig. 5e) (Lear et al., 2016; Farmer et al., 2019). The $\delta^{13}C_{corr}$ - ϵ_{Nd} relationship confirms the presence of glacial deep waters in the North and South Atlantic that contained more respired carbon, which is consistent with the reconstructions (Figs. 5e and 7). The carbon trapping in deep ocean affects the carbon cycle (Farmer et al., 2019; Khatiwala et al., 2019), by amplifying the nonlinear response of the climate system, which would have contributed to the shift from the 41 kyr world where the system responded linearly to the insolation forcing towards the highly nonlinear 100 kyr world (Chalk et al., 2017). Our results underscore the importance of physical processes (deep water formation, ventilation depths and strength, air/sea exchange) to modify the oceanic carbon storage (Lear et al., 2016; Farmer et al., 2019) in addition to biological carbon pumping (Chalk et al., 2017). The combination of foraminiferal authigenic ϵ_{Nd} with epibenthic $\delta^{13}C$ corrected for global-scale variability allow us to distinguish water mass mixing, NSW and SSW endmember modification and accumulation of respired carbon.

6. Conclusions

By combining ϵ_{Nd} recorded in planktonic foraminiferal authigenic fractions with *C. wuellerstorfi* $\delta^{13}C$ and $\delta^{18}O$ of cores from the Northeast (18°N, 3100 m water depth, MD03-2705) and the Southeast Atlantic Ocean (29°S, 1700 m water depth, ODP Site 1085), we investigated the relationship between the AMOC and oceanic carbon storage in the Atlantic Ocean over the past 1100 kyr. Our major findings are as follows.

Mechanical cleaning of foraminiferal shells of core MD03-2705 located under Saharan dust plume was revealed to be efficient. Glacial samples are more susceptible to be affected by Saharan dust and repeated ultrasonication successfully removed dust minerals to extract water ϵ_{Nd} signals.

Based on the compilation of foraminiferal ϵ_{Nd} records covering the 900-ka event and modelling results, the positive shift of reconstructed water ϵ_{Nd} values at the 900-ka event is estimated to have been produced by reduced AMOC with changes in the Nd source to the North Atlantic. In our model results, enhanced Southern Ocean overturning circulation alone cannot form the observed positive ϵ_{Nd} shift.

The relationship between foraminiferal ϵ_{Nd} and benthic $\delta^{13}C$ corrected for the effect of the global carbon cycle ($\delta^{13}C_{corr}$) reveals the presence of carbon-rich deep-water (>3000 m) in the South Atlantic as well as in the North Atlantic at the 900-ka event and during glacial periods. It contrasts well with the intermediate water masses of which ϵ_{Nd} and $\delta^{13}C_{corr}$ values can be essentially explained by a binary mixing of northern and southern source waters.

The depleted $\delta^{13}C_{corr}$ in the deep South Atlantic cannot be accounted solely for increased biological productivity by iron fertilization in the Southern Ocean. Reduced ventilation rate of deep NSW and SSW and/or air/sea exchange in the Southern Ocean played a key role, favouring carbon storage in the deep Atlantic.

This would have contributed to the establishment of strong glacial conditions in the 100 kyr world.

Data availability

Data of this study can be found in the supporting information and on Pangaea (www.pangaea.de).

Author contribution statement

Declaration of competing interest

The authors declare that they have no known competing financial interests or personal relationships that could have appeared to influence the work reported in this paper.

Acknowledgements

Appendix A. Supplementary data

Supplementary data to this article can be found online at https://doi.org/10.1016/j.quascirev.2020.106752.

References

Antonov, J.I., Seidov, D., Boyer, T.P., Locarnini, R.A., Mishonov, A.V., Garcia, H.E., Baranova, O.K., Zweng, M.M., Johnson, D.R., 2010. World ocean Atlas 2009, volume 2: salinity. In: Levitus, S. (Ed.), NOAA Atlas NESDIS 68. U.S. Government Printing Office, Washington, D.C., p. 184

Arsouze, T., Dutay, J.C., Kageyama, M., Lacan, F., Alkama, R., Marti, O., Jeandel, C., 2008. A modeling sensitivity study of the influence of the Atlantic meridional overturning circulation on neodymium isotopic composition at the Last Glacial Maximum. Clim. Past 4, 191−203.

Barker, S., Greaves, M., Elderfield, H., 2003. A study of cleaning procedures used for foraminiferal Mg/Ca paleothermometry. G-cubed 4 (9). https://doi.org/10.1029/2003GC000559.

Bell, D.B., Jung, S.J.A., Kroon, D., Lourens, L.J., Hodell, D.A., 2014. Local and regional trends in Plio-Pleistocene δ18O records from benthic foraminifera. G-cubed 15, 3304−3321.

Biastoch, A., Böning, C.W., Lutjeharms, J.R.E., 2008. Agulhas leakage dynamics affects decadal variability in Atlantic overturning circulation. Nature 456, 489.

Bickert, T., Wefer, G., 1996. Late Quaternary deep water circulation in the South Atlantic: reconstruction from carbonate dissolution and benthic stable isotopes. In: Wefer, G., Berger, W.H., Siedler, G., Webb, D. (Eds.), South Atlantic: Present and Past Circulation. Springer-Verlag, Berlin, pp. 599−620.

Bickert, T., Wefer, G., 1999. South Atlantic and benthic foraminifer δ^{13}C deviations: implications for reconstructing the Late Quaternary deep-water circulation. Deep Sea Res. Part II Top. Stud. Oceanogr. 46, 437−452.

Bickert, T., Wefer, G., Müller, P.J., 2003. Stable Isotopes and Sedimentology of Core GeoB1211-3. PANGAEA. https://doi.org/10.1594/PANGAEA.103634.

Boiteau, R., Greaves, M., Elderfield, H., 2012. Authigenic uranium in foraminiferal coatings: a proxy for ocean redox chemistry. Paleoceanography 27, PA3227.

Broecker, W.S., Peng, T.H., 1987. The role of $CaCO_3$ compensation in the glacial to interglacial atmospheric CO_2 change. Global Biogeochem. Cycles 1, 15−39.

Caley, T., Giraudeau, J., Malaizé, B., Rossignol, L., Pierre, C., 2012. Agulhas leakage as a key process in the modes of Quaternary climate changes. Proc. Natl. Acad. Sci. Unit. States Am. 109, 6835−6839.

Chalk, T.B., Hain, M.P., Foster, G.L., Rohling, E.J., Sexton, P.F., Badger, M.P.S., Cherry, S.G., Hasenfratz, A.P., Haug, G.H., Jaccard, S.L., Martínez-García, A., Pälike, H., Pancost, R.D., Wilson, P.A., 2017. Causes of ice age intensification across the Mid-Pleistocene Transition. Proc. Natl. Acad. Sci. Unit. States Am. 114, 13114−13119.

Chauvel, C., Blichert-Toft, J., 2001. A hafnium isotope and trace element perspective on melting of the depleted mantle. Earth Planet Sci. Lett. 190, 137−151.

Clark, P.U., Archer, D., Pollard, D., Blum, J.D., Rial, J.A., Brovkin, V., Mix, A.C., Pisias, N.G., Roy, M., 2006. The middle Pleistocene transition: characteristics, mechanisms, and implications for long-term changes in atmospheric pCO2. Quat. Sci. Rev. 25, 3150−3184.

Clark, P.U., Pollard, D., 1998. Origin of the middle pleistocene transition by ice sheet erosion of regolith. Paleoceanography 13, 1−9.

Cornuault, M., Tachikawa, K., Vidal, L., Guihou, A., Siani, G., Deschamps, P., Bassinot, F., Revel, M., 2018. Circulation changes in the eastern mediterranean sea over the past 23,000 Years inferred from authigenic Nd isotopic ratios. Paleoceanography and Paleoclimatology 33, 264−280.

Dausmann, V., Frank, M., Gutjahr, M., Rickli, J., 2017. Glacial reduction of AMOC strength and long-term transition in weathering inputs into the Southern Ocean since the mid-Miocene: evidence from radiogenic Nd and Hf isotopes. Paleoceanography 32, 265−283.

Dickson, A.J., Leng, M.J., Maslin, M.A., 2008. Mid-depth South Atlantic Ocean circulation and chemical stratification during MIS-10 to 12: implications for atmospheric CO2. Clim. Past 4, 333−344.

Dickson, A.J., Leng, M.J., Maslin, M.A., Röhl, U., 2010. Oceanic, atmospheric and ice-sheet forcing of South East Atlantic Ocean productivity and South African monsoon intensity during MIS-12 to 10. Quat. Sci. Rev. 29, 3936−3947.

Dyez, K.A., Hönisch, B., Schmidt, G.A., 2018. Early pleistocene obliquity-scale pCO$_2$ variability at ~1.5 million years ago. Paleoceanography and Paleoclimatology 33, 1270−1291.

Du, J., Haley, B.A., Mix, A.C., 2020. Evolution of the global overturning circulation since the last Maximum based on marine authigenic neodymium isotopes. Quat. Sci. Rev. 241, 106396.

Elderfield, H., Cooper, M., Ganssen, G., 2000. Sr/Ca in multiple species of planktonic foraminifera: implications for reconstructions of seawater Sr/Ca. G-cubed 1, 1999GC000031.

Elderfield, H., Ferretti, P., Greaves, M., Crowhurst, S., McCave, I.N., Hodell, D., Piotrowski, A.M., 2012. Evolution of ocean temperature and ice volume through the mid-pleistocene climate transition. Science 337, 704−709.

Farmer, J.R., Hönisch, B., Haynes, L.L., Kroon, D., Jung, S., Ford, H.L., Raymo, M.E., Jaume-Seguí, M., Bell, D.B., Goldstein, S.L., Pena, L.D., Yehudai, M., Kim, J., 2019. Deep Atlantic Ocean carbon storage and the rise of 100,000-year glacial cycles. Nat. Geosci. 12, 355−360.

Ford, H.L., Sosdian, S.M., Rosenthal, Y., Raymo, M.E., 2016. Gradual and abrupt changes during the mid-pleistocene transition. Quat. Sci. Rev. 148, 222−233.

Friedrich, T., Timmermann, A., Stichel, T., Pahnke, K., 2014. Ocean circulation reconstructions from εNd: a model-based feasibility study. Paleoceanography 29, 1003−1023.

Galaasen, E.V., Ninnemann, U.S., Kessler, A., Irvalı, N., Rosenthal, Y., Tjiputra, J., Bouttes, N., Roche, D.M., Kleiven, H.F., Hodell, D.A., 2020. Interglacial instability of north atlantic deep water ventilation. Science 367, 1485−1489.

Garcia-Solsona, E., Jeandel, C., Labatut, M., Lacan, F., Vance, D., Chavagnac, V., Pradoux, C., 2014. Rare earth elements and Nd isotopes tracing water mass mixing and particle-seawater interactions in the SE Atlantic. Geochem. Cosmochim. Acta 125, 351−372.

Gebbie, G., 2014. How much did glacial North Atlantic water shoal? Paleoceanography 29, 190−209.

Gildor, H., Tziperman, E., 2000. Sea ice as the glacial cycles' Climate switch: role of seasonal and orbital forcing. Paleoceanography 15, 605−615.

Goldstein, S.L., Pena, L.D., Yehudai, M., Seguí, M.J., Kim, J., Knudson, K.P., Basak, C., 2017. The Atlantic Meridional Overturning Circulation over Time: a Nd Isotope Perspective. AGU Fall Meeting, San Francisco. PP53C-03.

Gutjahr, M., Frank, M., Stirling, C.H., Keigwin, L.D., Halliday, A.N., 2008. Tracing the Nd isotope evolution of north atlantic deep and intermediate waters in the western North Atlantic since the last glacial Maximum from blake ridge sediments. Earth Planet Sci. Lett. 266, 61−77.

Hasenfratz, A.P., Jaccard, S.L., Martínez-García, A., Sigman, D.M., Hodell, D.A., Vance, D., Bernasconi, S.M., Kleiven, H.F., Haumann, F.A., Haug, G.H., 2019. The residence time of Southern Ocean surface waters and the 100,000-year ice age

cycle. Science 363, 1080−1084.

Higgins, J.A., Kurbatov, A.V., Spaulding, N.E., Brook, E., Introne, D.S., Chimiak, L.M., Yan, Y., Mayewski, P.A., Bender, M.L., 2015. Atmospheric composition 1 million years ago from blue ice in the Allan Hills, Antarctica. In: Proceedings of the National Academy of Sciences, pp. 6887−6891, 201420232.

Hodell, D., Venz, K.A., 1992. Toward a high-resolution stable isotopic record of the Southern Ocean during the Plio-Pleistocene (4.8 to 0.8 Ma). In: Kennett, J.P., Warnke, D.A. (Eds.), The Antarctic Paleoenvironment: A Perspective on Global Change, Part I. Antarct. Res. Ser. . American Geophysical Union, Washington, DC, pp. 265−310.

Hodell, D., Channell, J.E.T., 2016. Mode transitions in Northern Hemisphere glaciation: co-evolution of millennial and orbital variability in Quaternary climate. Clim. Past 12, 1805−1828.

Hodell, D.A., Venz, K.A., Charles, C.D., Ninnemann, U.S., 2003a. Pleistocene vertical carbon isotope and carbonate gradients in the South Atlantic sector of the Southern Ocean. G-cubed 4, 1004.

Hodell, D.A., Charles, C.D., Curtis, J.H., Graham Mortyn, P., Ninnemann, U.S., Venz, K.A., 2003b. (Table T4) Stable oxygen and carbon isotope ratios of benthic and planktonic foraminifers and carbonate concentrations of ODP Site 177-1090 in the Southern Ocean. In: Gersonde, R., Hodell, D.A., Blum, P. (Eds.), Proceedings of the Ocean Drilling Program, Scientific Results, vol. 177. Ocean Drilling Program), College Station, TX, pp. 1−26. https://doi.org/10.1594/PANGAEA.218131.

Hönisch, B., Hemming, N.G., Archer, D., Siddall, M., McManus, J.F., 2009. Atmospheric carbon dioxide concentration across the mid-pleistocene transition. Science 324, 1551−1554.

Hoogakker, B.A.A., Rohling, E.J., Palmer, M.R., Tyrrell, T., Rothwell, R.G., 2006. Underlying causes for long-term global ocean δ13C fluctuations over the last 1.20 Myr. Earth Planet Sci. Lett. 248, 15−29.

Howe, J.N.W., Huang, K.-F., Oppo, D.W., Chiessi, C.M., Mulitza, S., Blusztajn, J., Piotrowski, A.M., 2018. Similar mid-depth atlantic water mass provenance during the last glacial Maximum and heinrich stadial 1. Earth Planet Sci. Lett. 490, 51−61.

Howe, J.N.W., Piotrowski, A.M., Hu, R., Bory, A., 2017. Reconstruction of east−west deep water exchange in the low latitude Atlantic Ocean over the past 25,000 years. Earth Planet Sci. Lett. 458, 327−336.

Howe, J.N.W., Piotrowski, A.M., Noble, T.L., Mulitza, S., Chiessi, C.M., Bayon, G., 2016. North Atlantic deep water production during the last glacial Maximum. Nat. Commun. 7, 11765.

Hu, R., Piotrowski, A.M., Bostock, H.C., Crowhurst, S., Rennie, V., 2016. Variability of neodymium isotopes associated with planktonic foraminifera in the Pacific Ocean during the Holocene and last glacial Maximum. Earth Planet Sci. Lett. 447, 130−138.

Jaccard, S.L., Hayes, C.T., Martínez-García, A., Hodell, D.A., Anderson, R.F., Sigman, D.M., Haug, G.H., 2013. Two modes of change in Southern Ocean productivity over the past million years. Science 339, 1419−1423.

Jeandel, C., 1993. Concentration and isotopic composition of neodymium in the south Atlantic Ocean. Earth Planet Sci. Lett. 117, 581−591.

Jeandel, C., Arsouze, T., Lacan, F., Téchine, P., Dutay, J.-C., 2007. Isotopic Nd compositions and concentrations of the lithogenic inputs into the ocean: a compilation, with an emphasis on the margins. Chem. Geol. 239, 156−164.

Jorissen, F., Fontanier, C., Thomas, E., 2007. Paleoceanographical proxies based on deep-sea benthic foraminiferal assemblage characteristics. In: Hillaire-Marcel, C., de Vernal, A. (Eds.), Proxies in Late Cenozoic Paleoceanography. Elsevier, pp. 277−340.

Jullien, E., Grousset, F., Malaizé, B., Duprat, J., Sanchez-Goni, M.F., Eynaud, F., Charlier, K., Schneider, R., Bory, A., Bout, V., Flores, J.A., 2007. Low-latitude "dusty events" vs. high-latitude "icy Heinrich Events". Quat. Res. 68, 379−386.

Key, R.M., Kozyr, A., Sabine, C.L., Lee, K., Wanninkhof, R., Bullister, J.L., Feely, R.A., Millero, F.J., Mordy, C., Peng, T.H., 2004. A global ocean carbon climatology: results from global data analysis project (GLODAP). Global Biogeochem. Cycles 18, GB4031.

Khatiwala, S., Schmittner, A., Muglia, J., 2019. Air-sea disequilibrium enhances ocean carbon storage during glacial periods. Science Advances 5, eaaw4981.

Knorr, G., Lohmann, G., 2003. Southern Ocean origin for the resumption of Atlantic thermohaline circulation during deglaciation. Nature 424, 532.

Krueger, S., Leuschner, D.C., Ehrmann, W., Schmiedl, G., Mackensen, A., 2012. North Atlantic deep water and antarctic bottom water variability during the last 200ka recorded in an abyssal sediment core off South Africa. Global Planet. Change 80−81, 180−189.

Larqué, L., Maamaatuaiahutapu, K., Garçon, V., 1997. On the intermediate and deep water flows in the South Atlantic Ocean. J. Geophys. Res.: Oceans 102, 12425−12440.

Lear, C.H., Billups, K., Rickaby, R.E.M., Diester-Haass, L., Mawbey, E.M., Sosdian, S.M., 2016. Breathing more deeply: deep ocean carbon storage during the mid-Pleistocene climate transition. Geology 44, 1035−1038.

Lisiecki, L.E., Raymo, M.E., 2005. A Pliocene-Pleistocene stack of 57 globally distributed benthic δ18O records. Paleoceanography 20, 1−17.

Malaizé, B., Jullien, E., Tisserand, A., Skonieczny, C., Grousset, E.F., Eynaud, F., Kissel, C., Bonnin, J., Karstens, S., Martinez, P., Bory, A., Bout-Roumazeilles, V., Caley, T., Crosta, X., Charlier, K., Rossignol, L., Flores, J.-A., Schneider, R., 2012. The impact of African aridity on the isotopic signature of Atlantic deep waters across the Middle Pleistocene Transition. Quat. Res. 77, 182−191.

Marino, M., Maiorano, P., Flower, B.P., 2011. Calcareous nannofossil changes during the mid-pleistocene revolution: paleoecologic and paleoceanographic evidence

from North atlantic site 980/981. Palaeogeogr. Palaeoclimatol. Palaeoecol. 306, 58−69.

Martinez-Garcia, A., Rosell-Melé, A., Jaccard, S.L., Geibert, W., Sigman, D.M., Haug, G.H., 2011. Southern Ocean dust-climate coupling over the past four million years. Nature 476, 312−315.

McClymont, E.L., Sosdian, S.M., Rosell-Melé, A., Rosenthal, Y., 2013. Pleistocene sea-surface temperature evolution: early cooling, delayed glacial intensification, and implications for the mid-Pleistocene climate transition. Earth Sci. Rev. 123, 173−193.

Menviel, L.C., Spence, P., Skinner, L.C., Tachikawa, K., Friedrich, T., Missiaen, L., Yu, J., 2020. Enhanced mid-depth southward transport in the Northeast atlantic at the last glacial Maximum despite a weaker AMOC. Paleoceanography and Paleoclimatology 35, e2019PA003793.

Mix, A.C., Fairbanks, R.G., 1985. North Atlantic surface-ocean control of Pleistocene deep-ocean circulation. Earth Planet Sci. Lett. 73, 231−243.

Muglia, J., Skinner, L.C., Schmittner, A., 2018. Weak overturning circulation and high Southern Ocean nutrient utilization maximized glacial ocean carbon. Earth Planet Sci. Lett. 496, 47−56.

Naveira Garabato, A.C., Heywood, K.J., Stevens, D.P., 2002. Modification and pathways of Southern Ocean deep waters in the Scotia Sea. Deep Sea Res. Oceanogr. Res. Pap. 49, 681−705.

Orsi, A.H., Johnson, G.C., Bullister, J.L., 1999. Circulation, mixing, and production of antarctic bottom water. Prog. Oceanogr. 43, 55−109.

Pena, L.D., Goldstein, S.L., 2014. Thermohaline circulation crisis and impacts during the mid-Pleistocene transition. Science 345, 318−322.

Petrick, B., McClymont, E.L., Littler, K., Rosell-Melé, A., Clarkson, M.O., Maslin, M., Röhl, U., Shevenell, A.E., Pancost, R.D., 2018. Oceanographic and climatic evolution of the southeastern subtropical Atlantic over the last 3.5 Ma. Earth Planet Sci. Lett. 492, 12−21.

Pin, C., Santos Zalduegui, J.F., 1997. Sequential separation of light rare-earth elements, thorium and uranium by miniaturized extraction chromatography: application to isotopic analyses of silicate rocks. Anal. Chim. Acta 339, 79−89.

Piotrowski, A.M., Howe, J., Rennie, V., Clegg, J., Elderfield, H., 2015. Atlantic and Pacific Deep Ocean Circulation and Carbon Cycling Changes during the Mid-pleistocene Transition. Goldschmidt Conference. Abstract 2015.

Pöppelmeier, F., Blaser, P., Gutjahr, M., Jaccard, S.L., Frank, M., Max, L., Lippold, J., 2020. Northern-sourced water dominated the Atlantic Ocean during the last glacial Maximum. Geology. https://doi.org/10.1130/G47628.1.

Rahlf, P., Hathorne, E., Laukert, G., Gutjahr, M., Weldeab, S., Frank, M., 2020. Tracing water mass mixing and continental inputs in the southeastern Atlantic Ocean with dissolved neodymium isotopes. Earth Planet Sci. Lett. 530, 115944.

Raymo, M.E., Oppo, D.W., Curry, W., 1997. The Mid-Pleistocene climate transition: a deep sea carbon isotopic perspective. Paleoceanography 12, 546−559.

Raymo, M.E., Oppo, D.W., Flower, B.P., Hodell, D.A., McManus, J.F., Venz, K.A., Kleiven, K.F., McIntyre, K., 2004. Stability of North Atlantic water masses in face of pronounced climate variability during the Pleistocene. Paleoceanography 19.

Raymo, M.E., Ruddiman, W.F., Shackleton, N.J., Oppo, D.W., 1990. Evolution of Atlantic-Pacific δ13C gradients over the last 2.5 m.y. Earth Planet Sci. Lett. 97, 353−368.

Rempfer, J., Stocker, T.F., Joos, F., Dutay, J.-C., 2012. Sensitivity of Nd isotopic composition in seawater to changes in Nd sources and paleoceanographic implications. J. Geophys. Res.: Oceans 117, C12010.

Schlitzer, R., 2015. Ocean Data View.

Schmieder, F., von Dobeneck, T., Bleil, U., 2000. The Mid-Pleistocene climate transition as documented in the deep South Atlantic Ocean: initiation, interim state and terminal event. Earth Planet Sci. Lett. 179, 539−549.

Schmittner, A., Gruber, N., Mix, A.C., Key, R.M., Tagliabue, A., Westberry, T.K., 2013. Biology and air-sea gas exchange controls on the distribution of carbon isotope ratios (δ13C) in the ocean. Biogeosciences 10, 5793−5816.

Skonieczny, C., McGee, D., Winckler, G., Bory, A., Bradtmiller, L.I., Kinsley, C.W., Polissar, P.J., De Pol-Holz, R., Rossignol, L., Malaizé, B., 2019. Monsoon-driven Saharan dust variability over the past 240,000 years. Science Advances 5, eaav1887.

Snyder, C.W., 2016. Evolution of global temperature over the past two million years. Nature 538, 226−228.

Stichel, T., Frank, M., Rickli, J., Haley, B.A., 2012. The hafnium and neodymium isotope composition of seawater in the Atlantic sector of the Southern Ocean. Earth Planet Sci. Lett. 317−318, 282−294.

Stichel, T., Hartman, A.E., Duggan, B., Goldstein, S.L., Scher, H., Pahnke, K., 2015. Separating biogeochemical cycling of neodymium from water mass mixing in the Eastern North Atlantic. Earth Planet Sci. Lett. 412, 245−260.

Tabor, C.R., Poulsen, C.J., 2016. Simulating the mid-Pleistocene transition through regolith removal. Earth Planet Sci. Lett. 434, 231−240.

Tachikawa, K., Arsouze, T., Bayon, G., Bory, A., Colin, C., Dutay, J.-C., Frank, N., Giraud, X., Gourlan, A.T., Jeandel, C., Lacan, F., Meynadier, L., Montagna, P., Piotrowski, A.M., Plancherel, Y., Pucéat, E., Roy-Barman, M., Waelbroeck, C., 2017. The large-scale evolution of neodymium isotopic composition in the global modern and Holocene ocean revealed from seawater and archive data. Chem. Geol. 457, 131−148.

Tachikawa, K., Athias, V., Jeandel, C., 2003. Neodymium budget in the modern ocean and paleo-oceanographic implications. J. Geophys. Res. 108, 3254.

Tachikawa, K., Piotrowski, A.M., Bayon, G., 2014. Neodymium associated with foraminiferal carbonate as a recorder of seawater isotopic signatures. Quat. Sci. Rev. 88, 1−13.

Tachikawa, K., Roy-Barman, M., Michard, A., Thouron, D., Yeghicheyan, D.,

Jeandel, C., 2004. Neodymium isotopes in the Mediterranean Sea: comparison between seawater and sediment signals. Geochem. Cosmochim. Acta 68, 3095−3106.

Tachikawa, K., Toyofuku, T., Basile-Doelsch, I., Delhaye, T., 2013. Microscale neodymium distribution in sedimentary planktonic foraminiferal tests and associated mineral phases. Geochem. Cosmochim. Acta 100, 11−23.

Tachikawa, K., Rapuc, W., Dubois-Dauphin, Q., Guihou, A., Skonieczny, C., 2020. Reconstruction of ocean circulation based on neodymium isotopic composition: potential limitations and application to the Mid-Pleistocene transition. Oceanography. https://doi.org/10.5670/oceanog.2020.205.

Talley, L.D., 2013. Closure of the global overturning circulation through the Indian, pacific, and southern oceans: schematics and transports. Oceanography 26 (1), 80−97.

Tanaka, T., Togashi, S., Kamioka, H., Amakawa, H., Kagami, H., Hamamoto, T., Yuhara, M., Orihashi, Y., Yoneda, S., Shimizu, H., Kunimaru, T., Takahashi, K., Yanagi, T., Nakano, T., Fujimaki, H., Shinjo, R., Asahara, Y., Tanimizu, M., Dragusanu, C., 2000. JNdi-1: a neodymium isotopic reference in consistency with LaJolla neodymium. Chem. Geol. 168, 279−281.

Tisserand, A., Malaizé, B., Jullien, E., Zaragosi, S., Charlier, K., Grousset, F., 2009. African monsoon enhancement during the penultimate glacial period (MIS 6.5 ~ 170 ka) and its atmospheric impact. Paleoceanography 24.

Venz, K.A., Hodell, D.A., 2002. New evidence for changes in plio−pleistocene deep water circulation from Southern Ocean ODP Leg 177 site 1090. Palaeogeogr. Palaeoclimatol. Palaeoecol. 182, 197−220.

Wefer, G., Berger, W.H., Richter, C., Shipboard_Scientific_Party, 1998. Site 1085 initial report. Proceedings of the Ocean Drilling Program, Scientific Results, Initial Reports 175, 385−428.

Willeit, M., Ganopolski, A., Calov, R., Brovkin, V., 2019. Mid-Pleistocene transition in glacial cycles explained by declining CO_2 and regolith removal. Science Advances 5, eaav7337.

Williams, T.J., 2018. Investigating the Circulation of Southern Ocean Deep Water Masses over the Last 1.5 Million Years by Geochemical Fingerprinting of Marine Sediments. Department of Earth Sciences. University of Cambridge, Cambridge (PhD thesis).

Yan, Y., Bender, M.L., Brook, E.J., Clifford, H.M., Kemeny, P.C., Kurbatov, A.V., Mackay, S., Mayewski, P.A., Ng, J., Severinghaus, J.P., Higgins, J.A., 2019. Two-million-year-old snapshots of atmospheric gases from Antarctic ice. Nature 574, 663−666.

Zhao, N., Oppo, D.W., Huang, K.-F., Howe, J.N.W., Blusztajn, J., Keigwin, L.D., 2019. Glacial−interglacial Nd isotope variability of North Atlantic Deep Water modulated by North American ice sheet. Nat. Commun. 10, 5773.

Zieringer, M., Frank, M., Stumpf, R., Hathorne, E.C., 2019. The distribution of neodymium isotopes and concentrations in the eastern tropical North Atlantic. Chem. Geol. 511, 265−278.